The relative importance of wind and hydroclimate drivers in modulating the interannual variability of dust emissions in Earth system models

Xinzhu Li[1], Longlei Li[2], Yan Feng[3], and Xin Xi[1]

[1]Department of Geological and Mining Engineering and Sciences, Michigan Technological University, Houghton, MI, USA
[2]Department of Earth and Atmospheric Sciences, Cornell University, Ithaca, NY, USA
[3]Environmental Science Division, Argonne National Laboratory, Lemont, IL, USA

Correspondence: Longlei Li (ll859@cornell.edu) and Xin Xi (xinxi@mtu.edu)

Abstract. Windblown dust emissions are governed by near-surface wind speed and soil erodibility, the latter modulated by hydroclimate and land use conditions. Accurate model representations of these drivers are essential for reproducing historical dust variability and projecting future dust changes. Recognizing the unobservable, model-specific nature of dust emission fluxes, this study evaluates the discrepancies among 21 Earth system models in representing the relative influences of wind speed versus hydroclimate drivers on the interannual variability of dust emissions. In the hyperarid climate zone, the models show poor agreement in simulated dust variability, with only 10% out of 210 pairwise comparisons showing significant positive correlations. In arid and semiarid zones, the models display a dual pattern driven by a "double-edged sword" effect of land surface memory: models with coherent hydroclimate variability show improved agreement, whereas those with divergent hydroclimate representations show larger disagreement. The models mostly capture the dominant wind control over the hyperarid zone, but show great discrepancies in the relative importance of wind versus hydroclimate drivers over arid and semiarid zones. GFDL-ESM4 and CESM2-CAM-Kok overestimate the hydroclimate influence in the hyperarid zone. Implementing the Kok et al. (2014) dust scheme in CESM and E3SM generally reduces wind contributions to dust variability, e.g., from 56% to 44% in CESM and from 86% to 74% in E3SM within the arid zone. These findings underscore the need to improve near-surface wind simulations in hyperarid areas and land surface process representations in arid and semiarid areas to reduce uncertainties in dust emission simulations.

1 Introduction

Windblown dust aerosol is an essential element of the Earth's biogeochemical cycle and has become a global concern due to its wide-ranging impacts on the climate, ecosystems, agriculture, and society. Dust emission is modulated by near-surface wind speed and the abundance and availability of fine soils, which collectively determine the timing, location, duration, and intensity of dust events (Xi, 2023). The most abundant fine sediments are typically found in low-relief areas with thick accumulations of unconsolidated materials produced by weathering, fluvial, and/or aeolian processes (Bryant, 2013). The sediment availability for dust production is influenced by environmental conditions such as surface soil moisture and armoring (e.g., vegetation, soil

crust) which determine the minimum or threshold wind velocity that must be reached to mobilize soil particles (Bullard et al., 2011). The environmental controls of dust emissions have been incorporated in Earth system models (ESMs) to project dust aerosol responses to climate variability and change. Specifically, the horizontal saltation flux is parameterized as the third or fourth power of wind speed, reflecting the dominant role of infrequent, high-wind events. Many ESMs use prescribed, time-invariant dust source functions to represent spatially varying sediment abundance, with high values assigned to low-relief areas which experience frequent dust activity as observed by satellites (Ginoux et al., 2001; Prospero et al., 2002; Zender et al., 2003). The sediment abundance is typically assumed to be unlimited without accounting for depletion or replenishment over time (Zhang et al., 2016). In ESMs, sediment availability is closely coupled with hydroclimate and land surface processes. Surface soil moisture, as simulated by land surface schemes, is directly used to determine the threshold wind velocity for saltation (e.g., Fécan et al., 1999). The bare soil fraction is used to exclude non-erodible surfaces covered by snow, ice, water bodies, or vegetation. Vegetation also increases the surface roughness and reduces the wind shear stress exerted on exposed soils (Marticorena and Bergametti, 1995; Shao et al., 2011). This effect can be represented using drag partitioning schemes but is currently not considered in most ESMs.

Numerous studies have evaluated the consistency and performance of current ESMs in simulating the global dust cycle under the Aerosol Comparisons between Observations and Models (AeroCom) initiative and Coupled Model Intercomparison Project (CMIP) (Textor et al., 2006; Huneeus et al., 2011; Kim et al., 2014; Wu et al., 2020; Gliß et al., 2021; Zhao et al., 2022; Kim et al., 2024). Overall, modern-day dust aerosol column burden is reasonably constrained by ground- and satellite-based aerosol optical depth (AOD) observations, leading to better model agreement than that in dust emission and deposition estimates. Knippertz and Todd (2012) suggested that model tuning to match satellite observations, e.g., via the use of prescribed dust source functions, induces a compensational effect between dust emission and deposition, both of which lack robust observational constraints at the global scale. Indeed, past studies have reported persistent, substantial model discrepancies in global dust emission estimates and difficulties in reproducing the historical dust variability and its dependence on wind speed and bare soil fraction (Huneeus et al., 2011; Evan et al., 2014; Evan, 2018; Pu and Ginoux, 2018; Wu et al., 2020; Gliß et al., 2021; Zhao et al., 2022). More recently, Kok et al. (2023) suggested that current ESMs failed to capture the large increase of global dust burden since preindustrial times, likely due to inaccurate representations of the climate and land-use drivers of dust emissions, and/or the dust sensitivity to these drivers in these models.

The model discrepancies can be explained, at least in part, by the choice of dust emission schemes. Earlier schemes rely on prescribed, time-invariant dust source functions to shift emissions towards satellite-observed hotspot regions (Ginoux et al., 2001; Zender et al., 2003), whereas newer schemes adopt more mechanistic approaches that represent sediment availability as a function of land surface conditions, thereby eliminating the need for prescribed source functions (Kok et al., 2014b). With improved model physics, however, newer schemes require a larger set of input parameters that may introduce additional uncertainties. In addition, some schemes explicitly represent sandblasting efficiency to describe the momentum transfer from salting soil grains to dust entrainment into the atmosphere (e.g., Zender et al., 2003; Kok et al., 2014b), while simplified approaches assume a linear scaling between the vertical and saltation dust fluxes (e.g., Ginoux et al., 2001; Volodin and Kostrykin, 2016). The choice of wind speed also varies: some schemes use 10-m winds for simplicity, while others use friction

velocity, which more accurately captures the wind stress acting on soil surfaces but requires information on surface roughness. Because surface roughness length is poorly constrained by observations, models rely on varying assumptions and tunings to account for its effects on dust emissions (e.g., Peng et al., 2012; Albani et al., 2015; Tegen et al., 2019).

Even when using the same dust scheme, ESMs can diverge substantially in dust emission simulations because of differences in model configurations (e.g., horizontal resolution, vertical levels), parameter tunings, and coupled physical parameterizations. For instance, the bare soil fraction is determined from land type, vegetation fraction, and snow area extent, all of which may differ across ESMs. In particular, vegetation cover may be prescribed from satellite climatology or simulated interactively within the model. Dust emission discrepancies may also result from differences in soil properties (e.g., hydraulic conductivity), soil column structure (e.g., number and thickness of layers), and hydrologic processes (e.g., precipitation, runoff, evaporation), which ultimately determine the surface soil moisture and erodibility. The soil moisture effect on threshold wind velocity is also treated in different ways, for example, in how models define the residue moisture level below which soil wetness is assumed to have no effect (e.g., Fécan et al., 1999; Ginoux et al., 2001; Evans et al., 2016; Volodin and Kostrykin, 2016). Moreover, ESMs differ in the parameterizations for convection and atmospheric boundary layer processes, both of which strongly influence the generation of peak low-level winds. Therefore, it is not surprising that dust emission estimates are strongly model-dependent, considering the tight coupling between dust emission and the broader model physics and configurations.

While model discrepancies in global dust emission estimates are well documented in past studies, a key question remains as to how consistently and accurately current ESMs capture the interannual variability of dust emissions and their sensitivity to physical drivers. Addressing this question is essential for understanding and reducing model uncertainties in projecting dust responses to future climate and land-use changes. In this study, we evaluate the interannual variability of dust emission fluxes and quantify the relative influence of near-surface wind and hydroclimate drivers simulated by a suite of state-of-the-art ESMs. Compared with previous work, our analysis shifts the focus from climatological means to temporal variability and moves beyond documenting uncertainties to diagnosing their physical origins, thereby providing new insights for improving dust emission representations in ESMs.

A major challenge in evaluating dust models is the lack of direct observational constraints on dust emission fluxes. While satellite-based dust AOD and in-situ dust concentration measurements provide valuable insights into dust variability (e.g., Prospero and Lamb, 2003; Zender and Kwon, 2005; Ginoux et al., 2012), they integrate the effects of emission, transport, and deposition, making it difficult to isolate the emission process (the focus of this study). Thus, rather than validating model performance against observations, we focus on diagnosing the inter-model consistency in dust emission variability across different climate zones (i.e., hyperarid, arid and semiarid). In contrast to previous studies, we treat dust emission flux as an unobservable, model-specific quantity in our study, similar to Koster et al. (2009)'s view of root-zone soil moisture. This perspective recognizes the fact that simulated dust emission fluxes cannot be directly validated with field observations, and are characterized by a dynamic range defined by each model's physical parameterizations, parameter uncertainties, and structural configurations. The true information content of model-simulated dust emission fluxes therefore lies not necessarily in their absolute magnitudes, but in their spatiotemporal variability and sensitivities to physical drivers.

Table 1. Summary of the Earth system models and aerosol reanalysis datasets considered in this study. Dust source function (DSF) column indicates whether a prescribed dust source function is used. Leaf area index (LAI) column indicates whether LAI is treated as a prognostic variable. D_m, dust particle diameter upper limit.

Model	Resolution	D_m	Wind	DSF	LAI	Dust Scheme	Reference
CESM2-WACCM-Zender	0.9°×1.25°	10	u_*^3	Y	Y	Zender et al. (2003)	Gettelman et al. (2019)
CESM2-CAM-Zender	0.9°×1.25°	10	u_*^3	Y	Y	Zender et al. (2003)	Albani et al. (2015)
CESM2-CAM-Kok	0.9°×1.25°	10	u_*^3	N	Y	Kok et al. (2014b)	Li et al. (2022)
E3SM2-Zender	1°×1°	10	u_*^3	Y	N	Zender et al. (2003)	Feng et al. (2022)
E3SM3-Kok	1°×1°	10	u_*^3	Y	Y	Kok et al. (2014b)	Xie et al. (2025)
CanESM5-1	2.8°×2.8°	Bulk	u_*^3	Y	Y	Peng et al. (2012)	Sigmond et al. (2023)
CNRM-ESM2.1	1.4°×1.4°	20	u_*^3	N	Y	Tegen et al. (2002)	Séférian et al. (2019)
EC-Earth3-AerChem	2°×3°	20	u_*^3	Y	N	Tegen et al. (2002)	Van Noije et al. (2021)
GISS-E2.1-OMA	2°×2.5°	32	u_{10}^3	Y	N	Miller et al. (2006)	Miller et al. (2021)
GISS-E2.1-MATRIX	2°×2.5°	32	u_{10}^3	Y	N	Miller et al. (2006)	Miller et al. (2021)
GISS-E2.2-OMA	2°×2.5°	32	u_{10}^3	Y	N	Miller et al. (2006)	Rind et al. (2020)
GFDL-ESM4	1°×1.25°	20	u_*^3	Y	Y	Ginoux et al. (2001)	Shevliakova et al. (2024)
HadGEM3-GC31	0.6°×0.8°	63	u_*^3	Y	N	Woodward (2011)	Roberts et al. (2019)
UKESM1.0	1.25°×1.9°	63	u_*^3	N	Y	Woodward (2001)	Woodward et al. (2022)
INM-CM5.0	1.5°×2°	Bulk	u_*^4	N	N	Volodin and Kostrykin (2016)	Volodin (2022)
IPSL-CM6A-LR	1.26°×2.5°	Bulk	u_{10}^3	Y	Y	Balkanski et al. (2004)	Lurton et al. (2020)
MRI-ESM2.0	1.9°×1.9°	20	u_*^3	N	N	Shao et al. (1996)	Yukimoto et al. (2019)
MIROC6	1.4°×1.4°	10	u_{10}^3	N	Y	Takemura et al. (2009)	Tatebe et al. (2019)
MIROC-ES2L	2.8°×2.8°	10	u_{10}^3	N	Y	Takemura et al. (2009)	Hajima et al. (2020)
MPI-ESM-1.2	1.9°×1.9°	Bulk	u_*^3	Y	Y	Cheng et al. (2008)	Mauritsen et al. (2019)
NorESM2	0.9°×1.25°	10	u_*^3	Y	N	Zender et al. (2003)	Seland et al. (2020)
MERRA2	0.5°×0.63°	20	u_{10}^3	Y	N	Ginoux et al. (2001)	Randles et al. (2017)
JRAero	1.1°×1.1°	20	u_*^3	N	N	Shao et al. (1996)	Yumimoto et al. (2017)

The remainder of this paper is organized as follows. Section 2 describes the ESMs and reanalysis datasets considered in this study, and the dominance analysis technique used to quantify the joint and relative influences of dust emission drivers. Section 3 presents the model comparison of dust interannual variability and relative influence of wind and hydroclimate drivers. Section 4 summarizes the main conclusions.

2 Data and Approach

2.1 ESMs and aerosol reanalysis

We consider a total of 21 ESMs, summarized in Table 1. These include 18 models from the CMIP6 fully coupled historical experiment (1980–2014). For each model, we use the first ensemble member (r1i1p1f1) unless otherwise stated. Two CESM variants employ the dust emission parameterization of Zender et al. (2003) (hereafter the Zender scheme) but use different atmospheric schemes: the Community Atmosphere Model (CESM2-CAM-Zender) versus the Whole Atmosphere Community Climate Model (CESM2-WACCM-Zender). We also performed a separate CESM simulation (2004–2013) coupled with the dust scheme of Kok et al. (2014b) (hereafter the Kok scheme; CESM2-CAM-Kok) (Li et al., 2022). In addition, we conducted two experiments using the DOE E3SM model (1980–2014), which are coupled with the Zender (E3SM2-Zender) and Kok schemes (E3SM3-Kok), respectively (Feng et al., 2022; Xie et al., 2025). A key difference between the Zender and Kok schemes is that, the Zender scheme relies on a prescribed, time-invariant dust source function to shift emissions towards contemporary dust source areas, whereas the Kok scheme applies more physically based parameterizations of the dust sensitivity to soil erosion thresholds, thereby improving dust simulations without the use of prescribed source functions (Kok et al., 2014a). These paired CESM and E3SM experiments allow us to evaluate how the choice of dust emission schemes and host models affect the simulated dust sensitivities to physical drivers. However, it is worth noting that CESM2-CAM-Zender does not account for dust mineralogy, whereas CESM2-CAM-Kok simulates dust as mineral components with observationally constrained mineral optical properties (Li et al., 2024). This may lead to different radiative feedback on meteorology and contribute to model disparity in dust emissions. Similarly, E3SM3 incorporates extensive model updates relative to E3SM2, which may affect simulations of near-surface meteorological and land surface conditions relevant to dust emissions (Xie et al., 2025).

Several other model families share common heritage but differ in physics options and configurations. For example, three GISS-E2 models use the same dust scheme of Miller et al. (2006) but differ in model version (2.1 vs. 2.2) and aerosol microphysics scheme: One-Moment Aerosol (OMA; ensemble member r1i1p3f1) versus Multiconfiguration Aerosol TRacker of mIXing state (MATRIX; ensemble member r1i1p5f1) (Miller et al., 2021; Rind et al., 2020). UKESM1.0 is developed based on the HadGEM3-GC3.1 general circulation model. They use the same dust scheme of Woodward (2001) but differ in parameter tunings and dust source representations (Woodward et al., 2022). Both MIROC-ES2L and MIROC6 use the dust scheme from the SPRINTARS aerosol module (Takemura et al., 2009). MIROC-ES2L builds upon the MIROC general circulation model version 5.2 (MIROC5) (Hajima et al., 2020), while MIROC6 incorporates updated physics that improved the mean climate state and internal variability compared to MIROC5 (Tatebe et al., 2019).

We further compare the ESM simulations with two aerosol reanalysis products: Modern-Era Retrospective Analysis for Research and Applications version 2 (MERRA2, 1980–2014) (Gelaro et al., 2017), and Japanese Reanalysis for Aerosol (JRAero, 2011–2017) (Yumimoto et al., 2017). Dust emission in MERRA2 is simulated using the Ginoux et al. (2001) parameterization within the GOCART aerosol module of the GEOS-5 model. In JRAero, dust emissions are simulated using the Shao et al. (1996) energy-based scheme (same as in MRI-ESM2.0) within the Japan Meteorological Agency MASINGAR mk-2 global aerosol transport model (Yumimoto et al., 2017; Yukimoto et al., 2019). In both MERRA2 and JRAero, the meteorological

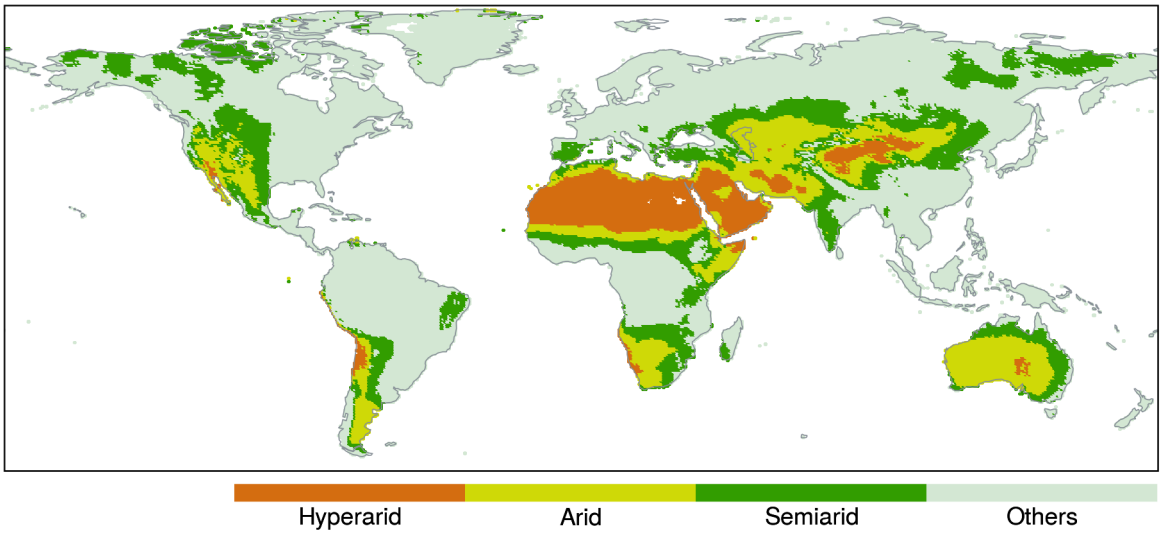

Figure 1. Definitions of hyperarid, arid, and semiarid climate zones.

inputs for dust emission calculations are generated via data assimilation of diverse in situ and remote sensing observations (including surface and upper-air wind measurements), which improves the accuracy of near-surface winds compared to free-running models (Gelaro et al., 2017; Yumimoto et al., 2017). The surface soil moisture in MERRA2 also benefits from the assimilation of observation-corrected precipitation. Although both reanalyses assimilate bias-corrected total AOD, it is expected to have limited effect on dust emission simulations.

We evaluate the consistency among the ESMs and reanalysis products in simulating the interannual variability of dust emission fluxes. To facilitate regionally consistent comparisons, global dryland areas are categorized into three climate zones—hyperarid, arid, and semiarid—based on aridity index (AI), defined as the ratio of climatological mean precipitation to potential evapotranspiration for 1970–2000 following (Zomer et al., 2022). The hyperarid zone is defined as $AI \leq 0.05$, arid zone as $0.05 < AI \leq 0.2$, and semiarid zone as $0.2 < AI \leq 0.5$. As shown in Figure 1, hyperarid areas primarily cover North Africa, Arabian Peninsula, Iranian Plateau, and Tarim Basin. Arid and semiarid areas cover other major dust sources, including the Sahel (North Africa), Turan Depression (Central Asia), Gobi Desert (East Asia), Thar Desert (South Asia), Kalahari Desert (Southern Africa), Chihuahua Desert (North America), Patagonia steppe (South America), and the Great Sandy and Simpson Deserts (Australia). The rationale for climate zone analysis is that the relative importance of wind versus hydroclimate controls on dust emission is expected to vary with climate aridity. Hyperarid areas are dominated by permanently dry, barren surfaces with minimal hydroclimate variability, so dust emission is primarily controlled by wind speed. In contrast, arid and semiarid zones experience greater precipitation and hydroclimate fluctuations, which exert stronger influences on soil erodibility.

2.2 Dominance analysis technique

Previous studies have commonly used linear regression coefficients to quantify the dust sensitivity to physical drivers (e.g., Pu and Ginoux, 2016; Aryal and Evans, 2021; Zhao et al., 2022). In multiple linear regression, a regression coefficient represents the mean change in the response variable (e.g., dust emission flux or AOD) associated with a unit change in a given predictor, while holding all other predictors constant. This interpretation assumes mutual independence among predictors, an assumption violated by strong correlations among hydroclimate variables. As a result, linear regression coefficients can yield misleading inference regarding the relative importance of predictors. Moreover, regression coefficients, standardized or not, may not provide a consistent basis for comparing predictor importance across the ESMs, due to inconsistent dynamic ranges of predictors among models.

In this study, we apply the dominance analysis technique to quantify the relative influence of wind and hydroclimate drivers on dust emissions. Dominance analysis quantifies the marginal contribution of each predictor to the total explained variance (R^2) in the response variable by evaluating all possible subset models ($2^p - 1$ subsets for p predictors) in a multiple linear regression framework (Budescu, 1993; Azen and Budescu, 2003). For each predictor, the method calculates its average incremental contribution to the total R^2 across all subset models of the same size (i.e., models with the same number of predictors). These incremental R^2 values are then averaged to obtain the predictor's overall contribution to the total R^2. A key feature of this approach is that the sum of individual predictor contributions equals the total R^2 of the full model (i.e., with all predictors included), thereby allowing the partitioning of explained variance among correlated predictors. The resulting predictor R^2 values thus represent the proportions of total variance in the response variable that can be attributed to each predictor, accounting for their multicollinearity.

The monthly dust emission fluxes simulated by each ESM are used as the response variable. Although the models differ in how the total emission flux is partitioned into discrete size bins—a key factor influencing dust transport and atmospheric lifetime—the size partitioning has minor effects on diagnosing the emission process itself. In particular, the physical drivers considered here operate upstream of the size partitioning, and thus mainly control the initiation and magnitude of total dust emission rather than its size-resolved characteristics.

For each ESM, we consider six predictors: 10-m wind speed, total precipitation (including liquid and solid phases), water content in the uppermost soil layer (soil moisture), 2-m specific humidity, 2-m air temperature, and leaf area index (LAI). These predictors are chosen because they are either directly used as input parameters in dust flux parameterizations or are closely linked to dust emission intensity, as suggested in previous studies (e.g., Engelstaedter et al., 2003; RAVI et al., 2006; Zou and Zhai, 2004; Sokolik et al., 2021; Cowie et al., 2015; Kim and Choi, 2015; Xi and Sokolik, 2015a, b; Xi, 2023). Among them, 10-m wind speed represents the wind shear drag responsible for dust mobilization, while the remaining variables represent the hydroclimate controls on sediment availability. Dominance analysis is applied to all ESMs and MERRA2 over grid cells with nonzero emissions. Prior to analysis, the data are first deseasonalized by subtracting month-wise climatological means from both the dust emission fluxes and predictors, and subsequently normalized to the 0–1 range via min-max scaling. The resulting grid-level predictor R^2 values are then used to assess (1) the internal spatial variability of predictor importance within each

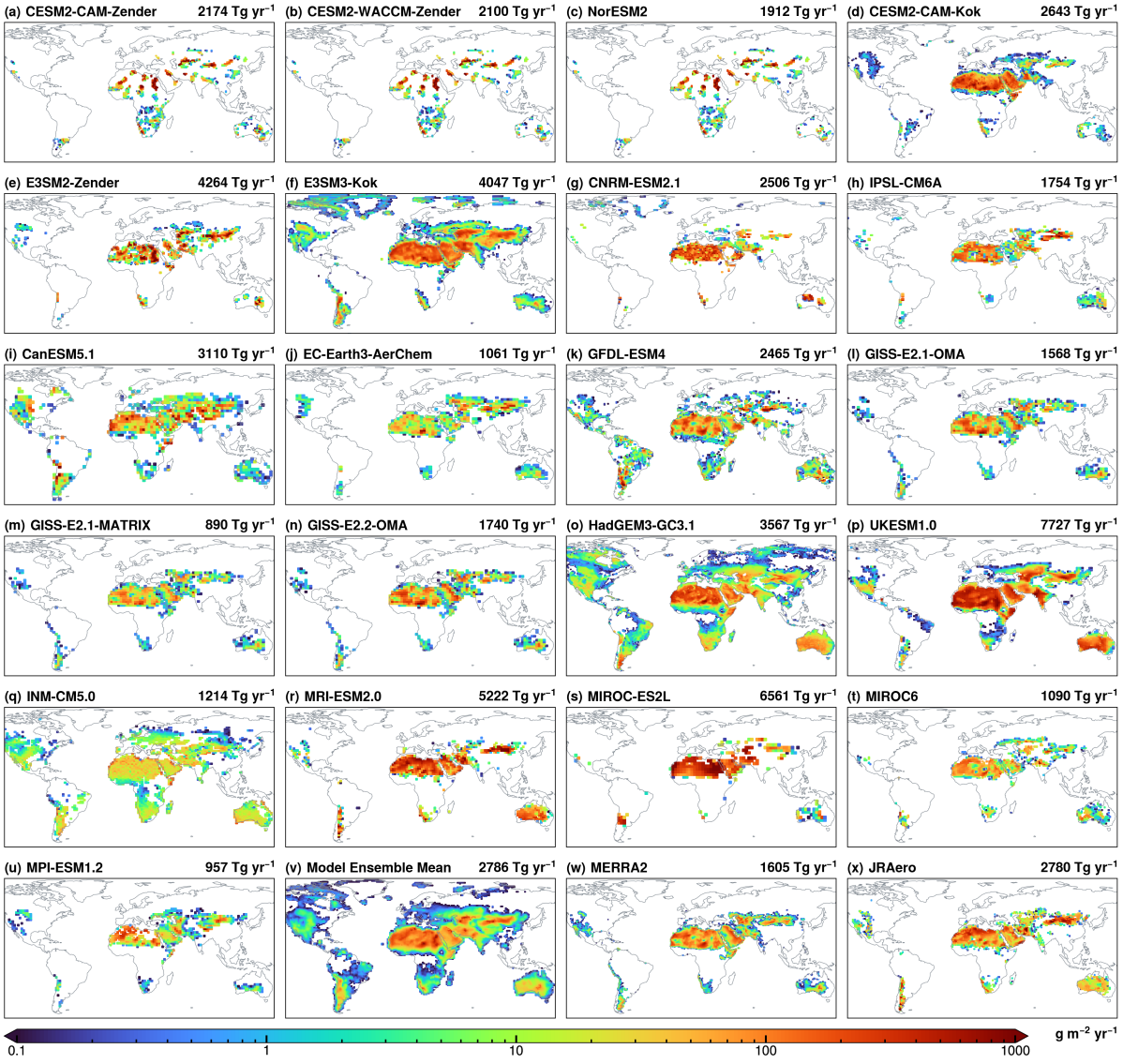

Figure 2. Climatological mean dust emission fluxes from (a–u) 21 Earth system models, (v) model ensemble mean, (w) MERRA2 reanalysis, and (x) JRAero reanalysis. Global annual total emissions are displayed on each panel.

climate zone and model, and (2) and inter-model consistency in representing the predictor relative influence on the interannual dust emission variability. JRAero is excluded from this analysis due to missing predictor data.

3 Results

3.1 Climatological distribution

Figure 2 displays the climatological mean annual dust emission fluxes from the 21 ESMs, their ensemble mean, and the MERRA2 and JRAero reanalyses for 2005–2014 (2004–2013 for CESM2-CAM-Kok and 2011–2017 for JRAero). All datasets capture the global dust belt stretching from West Africa across the Middle East to East Asia, as well as weaker sources in the Americas and Australia. Among the models, E3SM3-Kok and HadGEM2-GC31 simulate the most extensive dust-emitting areas, extending into high-latitude and subhumid areas. CESM2-CAM-Zender, CESM2-WACCM-Zender and NorESM2 restrict emissions to regions where the dust source function exceeds 0.1, resulting in discrete and spatially limited emission areas. Conversely, E3SM2-Zender employs the original dust source function of Zender et al. (2003), producing a more spatially continuous emission pattern (Fig. 2e).

Global annual dust emissions simulated by the ESMs vary greatly, ranging from 890 to 7727 Tg yr^{-1} with nearly an order of magnitude difference (Fig. 2a–2u). The ensemble mean estimate (Fig. 2v) is 2786 Tg yr^{-1} with a standard deviation of 1821 Tg yr^{-1}, corresponding to a diversity of 65% (defined as the ratio of the standard deviation to the ensemble mean). Based on models with an upper particle size limit of 20 μm, global emissions vary from 1062 to 6561 Tg yr^{-1}, with a mean of 3012 Tg yr^{-1} and diversity of 51%. Compared to aerosol reanalysis data, the ensemble mean estimate is close to JRAero (2780 Tg yr^{-1}, Fig. 2x), but considerably higher than MERRA2 (1605 Tg yr^{-1}, Fig. 2w). Also, the ensemble mean exhibits a more spatially homogeneous pattern over North Africa and the Arabian Peninsula, whereas MERRA2 and JRAero display more heterogeneous and localized emission patterns.

The model discrepancies in dust emission magnitude is consistent with previous assessments. For example, Huneeus et al. (2011) compared 14 AeroCom Phase I models and reported a global dust emission range of 500–4400 Tg yr^{-1} (diversity=58%), of which seven using a 20 μm upper size limit yielded 980–4300 Tg yr^{-1} (diversity=46%). Similarly, Gliß et al. (2021) compared 14 AeroCom Phase III models and reported a range of 850–5650 Tg yr^{-1} with a diversity of 64%. Based on 15 CMIP5 models Wu et al. (2020) reported a range of 740–8200 Tg yr^{-1} (diversity=66%), with seven models using particle diameters up to 20 μm producing 740–3600 Tg yr^{-1} (diversity=43%). More recently, Zhao et al. (2022) examined 15 CMIP6 AMIP models and reported a range of 1400–7600 Tg yr^{-1} (diversity=61%). Collectively, these studies, along with our results, demonstrate persistent large model uncertainties in global dust emission estimates, despite advances in model resolutions parameterizations, and process understanding.

Figure 3 displays the contributions of different climate zones to global dust emissions. The hyperarid zone accounts for more than half of global emissions in all models except CanESM5.1 and INM-CM5.0, both of which simulate relatively uniform emission patterns with less than 50% from hyperarid areas (Fig. 2i, 2q). This may be caused by known model deficiencies. As noted in Sigmond et al. (2023), improper parameter tunings related to the hybridization of dust tracers caused spurious dust events and inaccurate dust distributions in CanESM5.1. An interpolation error in the bare soil fraction also distorted the model's dust source characterization, resulting in poor agreement with satellite observations. In INM-CM5.0, the vertical dust flux is calculated as a function of wind velocity only, without accounting for land surface controls on the erosion threshold

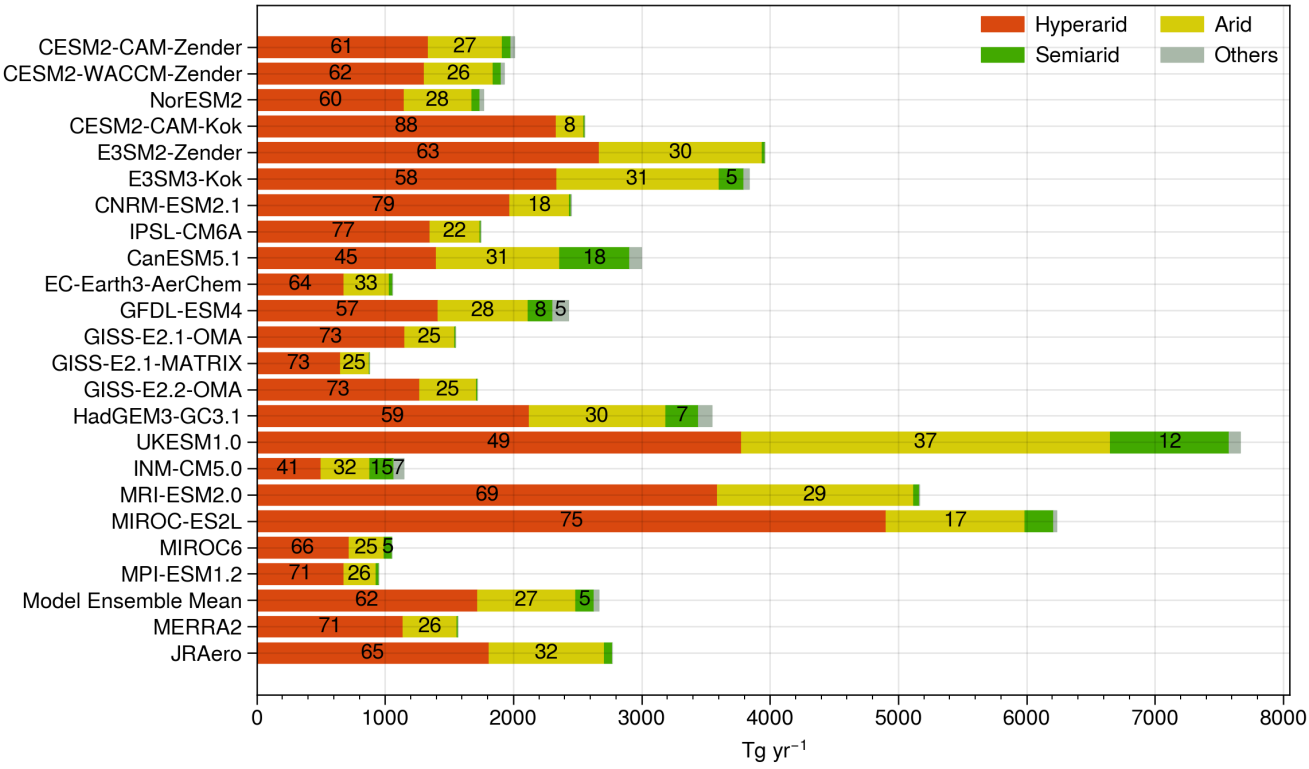

Figure 3. Contributions of different climate zones to global annual dust emissions. Numbers indicate percentages above 5%.

(Volodin and Kostrykin, 2016; Volodin, 2022). While this simplification may be appropriate for hyperarid climate zone, it can overestimate dust emissions over arid and semiarid zones where increased soil wetness and armoring suppress dust mobilization.

The contribution of the arid climate zone ranges from 8% (CESM2-CAM-Kok) to 37% (UKESM-1.0), indicating substantial model discrepancies compared to the hyperarid zone. The discrepancies become even larger over the semiarid zone, where the emission fraction ranges from less than 1% to 18%. Particularly, three models allocate more than 10% to the semiarid zone: CanESM5.1 (18%), INM-CM5.0 (15%), and UKESM1.0 (12%). Overall, as the climate regime transitions from hyperarid to semiarid, model-estimated dust source strengths become less consistent, revealing increasing uncertainty in how ESMs represent dust sensitivity to hydroclimate conditions.

Among the ESMs, CESM2-CAM-Zender and CESM2-WACCM-Zender produce nearly identical total emissions and spatial distributions, suggesting that the choice between CAM and WACCM atmospheric components has minimal effect. The paired CESM and E3SM experiments, however, show opposite tendencies: the hyperarid-zone contribution increases from 61% in CESM2-CAM-Zender to 88% in CESM2-CAM-Kok, but slightly decreases from 63% in E3SM2-Zender to 58% in E3SM3-Kok. The three GISS-E2 models produce consistent distributions across climate zones, although total emissions are about 40%

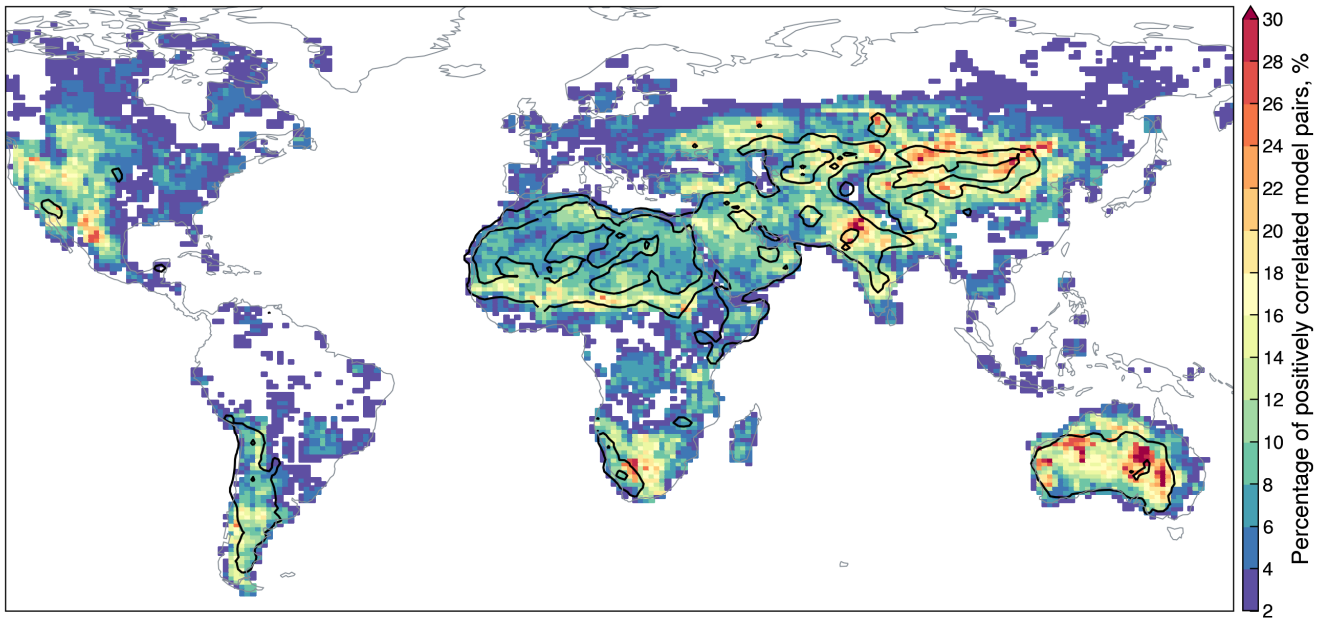

Figure 4. Percentage of statistically significant ($p \leq 0.1$), positive correlations out of every possible pairwise comparisons of deseasonalized monthly dust emission fluxes from 21 Earth system models. Black contours indicate the model ensemble mean emission flux of 10 and 100 Tg yr^{-1}.

lower when using the MATRIX aerosol scheme, possibly due to parameter tunings or underrepresentation of coarse dust (>5 μm diameter) in the MATRIX modal size distribution (Bauer et al., 2022).

UKESM1.0 emits nearly twice as much dust as HadGEM3-GC3.1, and exhibits slightly more uniform spatial distributions. As described in Woodward et al. (2022), UKESM1.0 is built upon HadGEM3-GC3.1 but applies parameter tunings that enhance friction velocity and suppress soil moisture, effectively increasing the wind gustiness and soil aridity leading to more emissions in UKESM1.0. The three Japanese models (MRI-ESM2.0, MIROC-ES2L, and MIROC6) also differ markedly in total emissions and, to a lesser extent, spatial distributions. MRI-ESM2.0 produces similar regional fractions to JRAero but nearly doubles the total emission magnitude. Despite using the same dust parameterization, MIROC-ES2L emits roughly five times more dust than MIROC6. This discrepancy can be largely explained by stronger winds in MIROC-ES2L, which produces 50% higher global mean wind speed than MIROC6. Moreover, MIROC6 prescribes non-zero LAI even in hyperarid areas, likely further suppressing dust generation relative to MIROC-ES2L (Hiroaki Tatebe, personal communications).

Based on the model ensemble mean, global dust emissions are partitioned as 61% from hyperarid, 27% from arid, and 5% from semiarid zones. In comparison, MERRA2 and JRAero allocate the vast majority of dust emissions to hyperarid and arid zones, with negligible contributions from the semiarid zone.

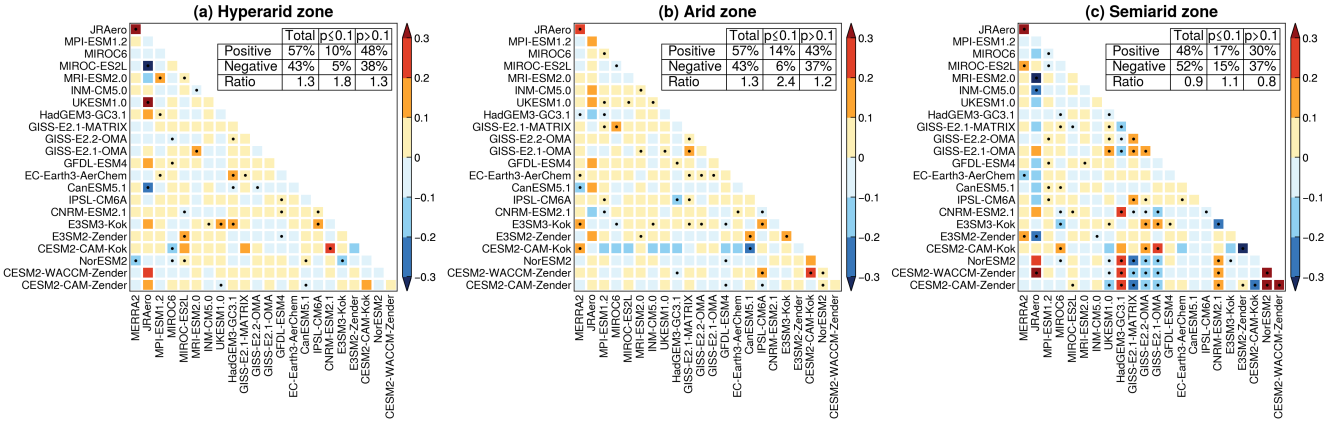

Figure 5. Spearman's rank correlation coefficients between dust emission flux anomalies averaged over hyperarid, arid, and semiarid climate zones. Dots indicate statistically significant correlations ($p \leq 0.1$). Summary tables are based on Earth system models only (MERRA2 and JRAero not included).

3.2 Interannual variability

This section evaluates the consistency among the ESMs in simulating the interannual variability of dust emissions. Monthly dust emission fluxes from all ESMs are first regridded to a common resolution of 0.9°×1.25° (the native grid of CESM2). To remove the influence of annual cycles, month-wise climatological means are subtracted from each grid cell, yielding deseasonalized dust emission flux anomalies. Spearman's rank correlation coefficients are then calculated between the monthly anomalies for every possible model pair. With 21 ESMs, this results in 210 pairwise comparisons. To quantify inter-model agreement, we calculate the percentage of model pairs exhibiting statistically significant ($p \leq 0.1$), positive correlations. A higher percentage indicates stronger inter-model agreement in simulating the dust variability, and vice versa. The results are displayed in Fig. 4.

Despite the dominant contributions to global dust emissions, the hyperarid climate zone exhibits generally poor inter-model agreement, with less than 10% of pairwise comparisons showing statistically significant positive correlations. Because dust emissions from hyperarid areas are predominantly controlled by near-surface wind speed, this poor agreement reflects inconsistencies in wind simulations among the ESMs. Indeed, we find that only 10% of model pairs produce positively correlated wind variability. Evan (2018) reported that dust-producing winds over the Sahara Desert are mainly driven by large-scale meteorological processes and that most CMIP5 models failed to capture the near-surface wind variability. These results indicate that improving the representation of near-surface winds is critical for reducing inter-model discrepancies in dust variability over hyperarid regions.

In contrast to the hyperarid zone, the arid and semiarid zones (such as the Sahel, South Asia, East Asia and Australia) exhibit significantly better agreement. To further assess how model consistency varies across climate regimes, Fig. 5 presents pairwise correlation matrices based on dust emission flux anomalies averaged over hyperarid, arid, and semiarid zones. The

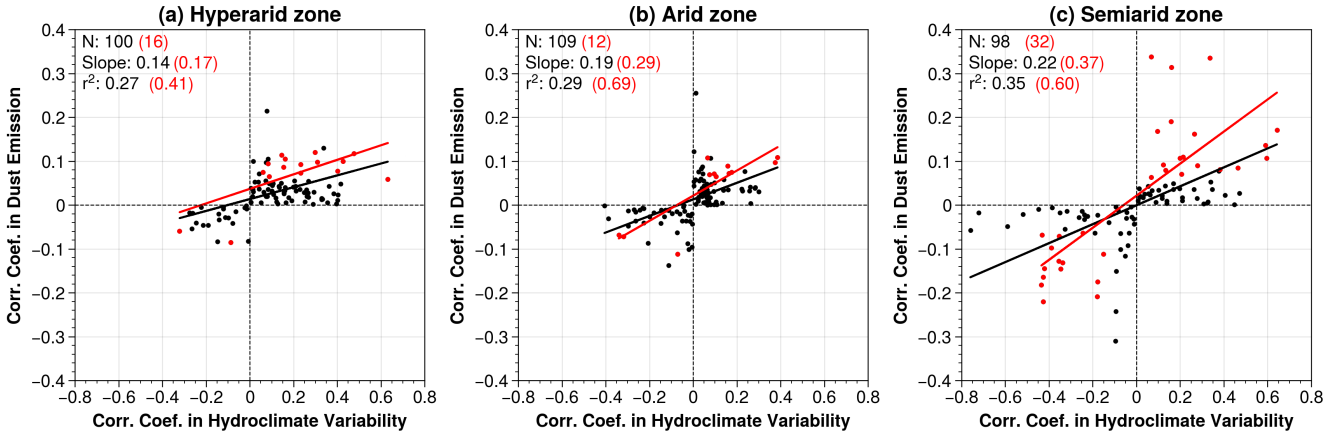

Figure 6. Statistical associations between pairwise model correlation coefficients ($p \leq 0.1$ shown in red) in dust emission fluxes and hydroclimate variability over (a) hyperarid, (b) arid, and (c) semiarid climate zones.

percentage of statistically significant, positively correlated model pairs increases from 10% in the hyperarid zone to 14% in the arid zone and 17% in the semiarid zone, indicating progressively better agreement where dust emissions are increasingly influenced by hydroclimate and land surface conditions. Meanwhile, the semiarid zone shows a larger percentage of negatively correlated model pairs (15%) than the hyperarid (5%) and arid (6%) zones. This dual pattern suggests that as the climate regime transitions from hyperarid to semiarid, the ESMs exhibit both stronger agreement and heightened disagreement in simulating the interannual variability of dust emissions.

This behavior can be explained by the strong influence of antecedent land surface conditions on soil erodibility in semiarid environments such as temperate grasslands and steppes (Shinoda et al., 2011; Nandintsetseg and Shinoda, 2015). In these regions, factors such as precipitation, soil moisture, and vegetation growth–decay cycles have lagged and long-lasting impacts on the availability of erodible sediments. For example, dry anomalies during the wet season such as reduced rainfall or earlier snowmelt can decrease soil cohesion and suppress vegetation growth, thereby prolonging bare soil exposure and enhancing the risk of wind erosion. This delayed response exemplifies the land surface memory effect, in which the slow adjustment of soil and vegetation conditions over weeks to months influences subsequent dust emissions long after the initial hydroclimate forcing (e.g., drought). We therefore hypothesize that the simultaneous increase in both model agreement and disagreement from hyperarid to semiarid zones reflects a "double-edged sword" effect of land surface memory: models with coherent representations of hydroclimate variability tend to converge in simulated dust variability (i.e., more positive correlations), whereas those with divergent hydroclimate representations diverge in the dust variability (i.e., more negative correlations).

To verify this hypothesis, we examine the statistical association between pairwise model correlations in dust emissions and those in hydroclimate variability. Specifically, we perform a principle component analysis (PCA) of the five hydroclimate variables (i.e., precipitation, soil moisture, specific humidity, air temperature, LAI) separately for the hyperarid, arid, and semiarid zones. The leading principle component (PC1), which explains at least 40% of the total variance in all zones, is

used as a proxy for the dominant hydroclimate variability. Spearman's rank correlation coefficients are then computed for all pairwise comparisons of deseasonalized monthly PC1 values, following the same approach as in Fig. 5.

Figure 6 compares the correlation coefficients for model pairs with the same sign (i.e., both positive or both negative) in dust emission fluxes and hydroclimate PC1. The regression slope and coefficient of determination (r^2) quantify the degree of statistical association between inter-model correlations in dust emission and hydroclimate variability. The positive relationships across all climate zones suggests that ESMs with stronger consensus in hydroclimate variability also tend to produce more consistent dust variability, and vice versa. More importantly, both the number of significantly correlated model pairs (N) and correlation strength (slope and r^2) show significant increases from hyperarid to semiarid zones. This result supports our speculation regarding the dual role of land surface memory: it enhances agreement among ESMs with coherent hydroclimate representations, while simultaneously amplifying disagreement among those with divergent hydroclimate variability.

3.3 Relative importance of wind and hydroclimate drivers

In this section, we present dominance analysis results on the collective and relative influence of wind and hydroclimate drivers on the simulated dust variability within each model. Figure 7 shows the total variance explained (R^2) by wind speed and five hydroclimate drivers (precipitation, soil moisture, specific humidity, air temperature, and LAI) in the ESMs and MERRA2. Results for CESM2-WACCM-Zender and NorESM2 are very similar to those of CESM2-CAM-Zender and thus not shown.

The ESMs show large discrepancies in the total R^2, reflecting inherent differences in the coupling strength between dust emission and physical drivers. When ranked by the global mean R^2, CanESM5.1 shows the lowest explanatory power of the predictors, followed by MPI-ESM1.2, MIROC6, and EC-Earth3-AerChem. The weak predictor–response relationship can be explained by several factors. Model deficiencies or errors (e.g., in CanESM5.1, Section 3.1) can weaken or distort the simulated relationships between dust emission and physical drivers. Simplified parameterizations and/or static land surface input can reduce the dust sensitivity to hydroclimate conditions. In addition, because dust emission is governed by highly nonlinear threshold processes, its dependence on the predictors may deviate from the linear assumptions underlying dominance analysis. As shown in Fig. 7, total R^2 values are generally lower in arid and semiarid areas than in hyperarid areas, likely due to increased nonlinearity in the dust-hydroclimate relationships that diminishes the explanatory power of multilinear regression models.

Despite these limitations, most ESMs produce significant total R^2 values over major dust sources, especially in hyperarid areas with R^2 above 0.5. Switching from the Zender to Kok dust scheme generally reduces R^2 in both CESM and E3SM (Fig. 7a–d). The GISS-E2 models show little differences between the OMA and MATRIX aerosol schemes, with a modest increase from version 2.1 to 2.2. UKESM1.0 and HadGEM3-GC3.1 show minimal differences, both showing high R^2 values globally. MIROC6 yields lower R^2 than MIROC-ES2L, particularly over hyperarid areas. MERRA2 produces higher R^2 than most ESMs, especially within arid and semiarid zones, indicating a stronger overall coupling between dust emissions and the selected predictors.

To assess the relative importance of wind and hydroclimate drivers, Fig. 8 presents the ratio of the wind speed-associated R^2 to the combined R^2 of the five hydroclimate variables. In all ESMs except GFDL-ESM4, this wind-to-hydroclimate R^2 ratio is well above 1 over hyperarid areas, consistent with the dominant control of wind speed on dust emission from persistently dry,

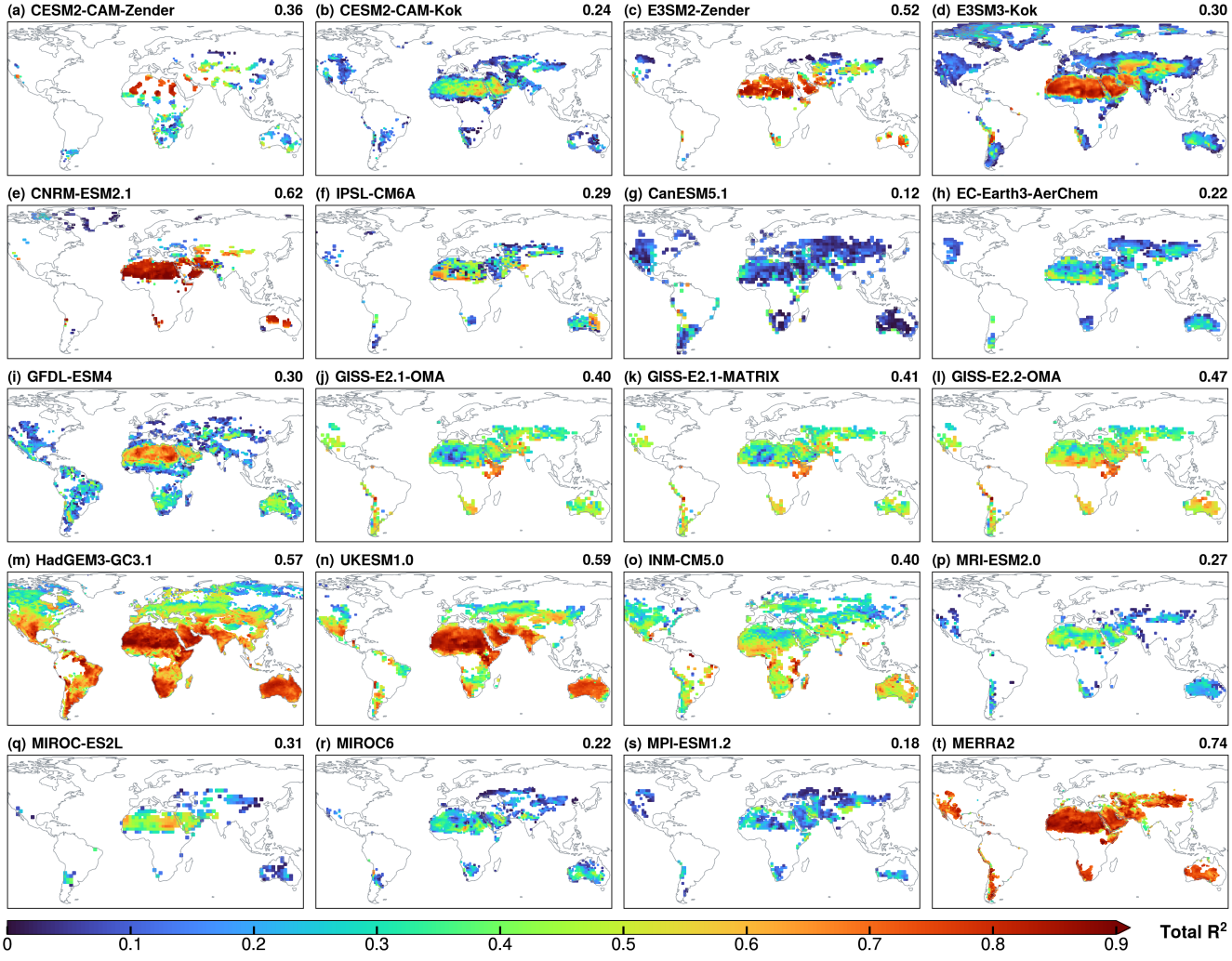

Figure 7. Total explained variance (R^2) in dust emission fluxes by six near-surface variables (wind speed, precipitation, soil moisture, specific humidity, air temperature and LAI) in Earth system models and MERRA2. Global mean R^2 values are shown on each panel.

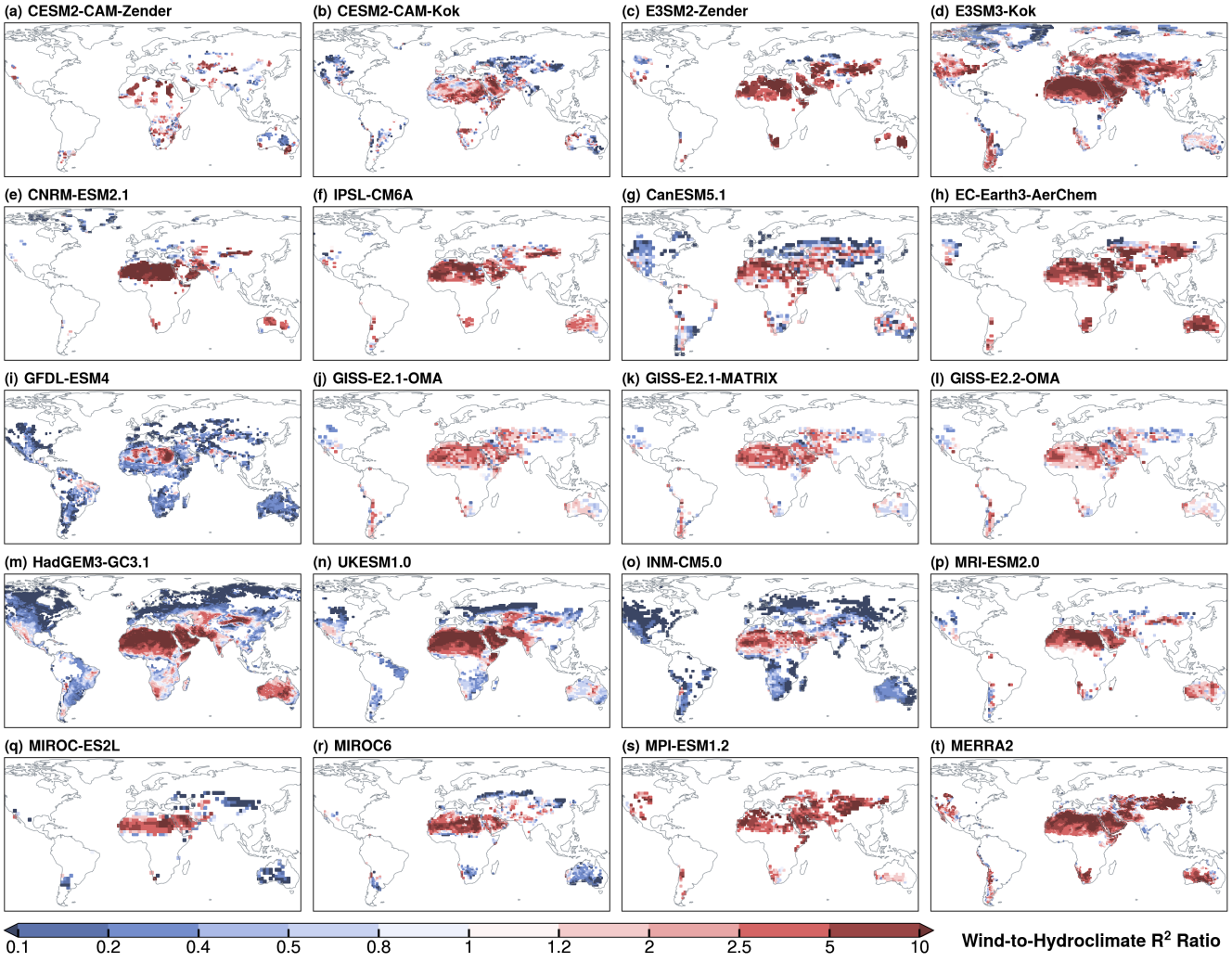

Figure 8. The ratio of wind speed-associated R^2 to the combined R^2 of five hydroclimate drivers (precipitation, soil moisture, specific humidity, air temperature and LAI) in Earth system models and MERRA2.

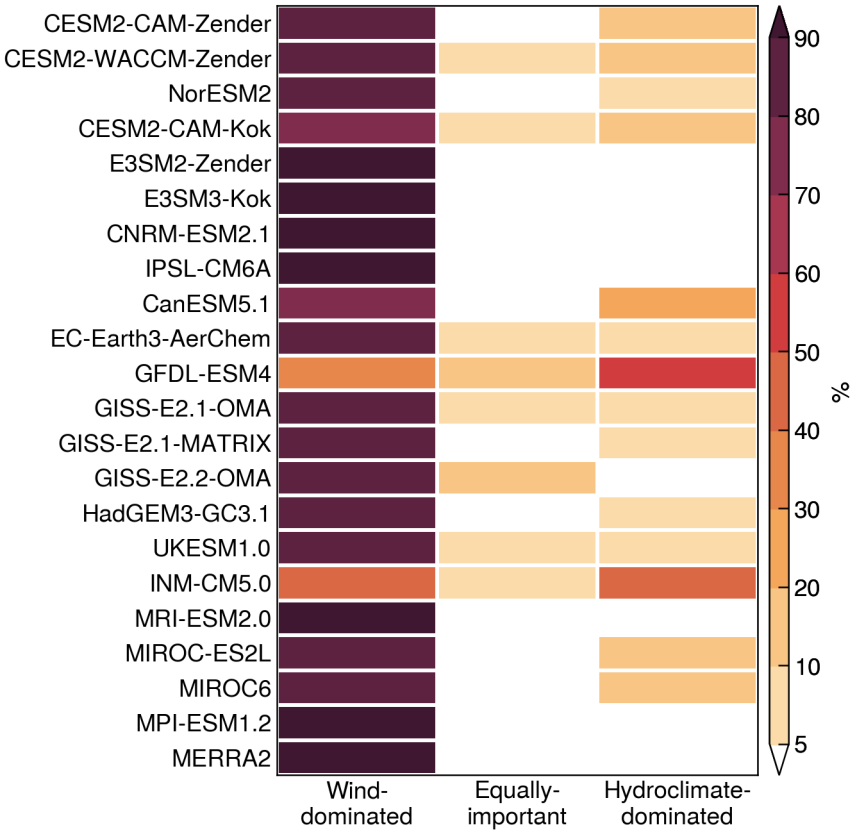

Figure 9. Fractional contributions of wind-dominated, equally-important, and hydroclimate-dominated regimes to global dust emissions in Earth system models and MERRA2.

barren surfaces. In contrast, arid and semiarid areas exhibit greater inter-model discrepancies, with ratios either above or below 1 depending on the model. This reflects substantial uncertainty in how models represent the relative influence of wind versus hydroclimate drivers in regions where hydroclimate and land surface conditions exert strong effects on sediment availability.

Based on the wind-to-hydroclimate R^2 ratios, we classify global dust-emitting areas into three regimes: wind-dominated (ratio$>$1.2), hydroclimate-dominated (ratio$<$0.8), and equally-important (0.8–1.2). Then we calculate the fractions of dust emitted from these regimes within each model. The results are displayed in Fig. 9. The ESMs show general agreement in the "equally-important" regime, with most models simulating less than 10% from regions where wind and hydroclimate drivers have nearly equal influence. GFDL-ESM4 produces the highest contribution (12%) in this regime.

The wind-dominated regime accounts for the majority of dust emissions (>80%) in most ESMs, consistent with the dominant contribution from hyperarid areas (Fig. 3). However, three models yield anomalously low estimates: GFDL-ESM4 (36%), INM-CM5.0 (43%) and CanESM5.1 (75%). These deviations can be explained by different reasons. As shown in Fig. 3, INM-CM5.0 and CanESM5.1 produce relatively homogeneous emission patterns, which reduce the fractional contribution from hyperarid

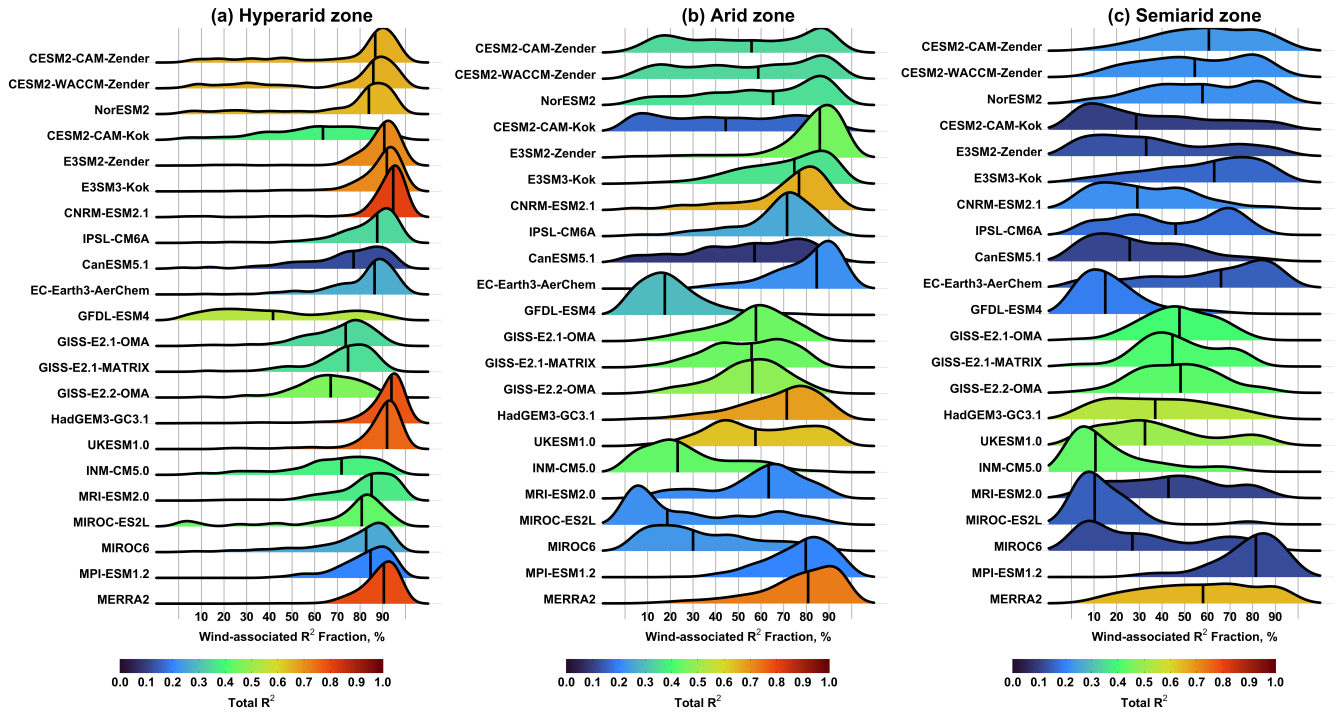

Figure 10. Ridgeline plots of the fractional contributions of wind speed to the total R^2 over (a) hyperarid, (b) arid, and (c) semiarid climate zones. Black vertical lines indicate median values. Color shading represent the mean total R^2 values.

or wind-dominated regions. In contrast, the low estimate in GFDL-ESM4 results from its anomalously strong hydroclimate influence over hyperarid areas. As shown in Fig. 8i, GFDL-ESM4 yields markedly low wind-to-hydroclimate ratios (<1) over North Africa, Arabian Peninsula, and Iranian Plateau, leading to the misclassification of these inherently wind-dominated regions as hydroclimate-dominated. Given the extremely scare precipitation and low hydroclimate variability in these regions, such strong hydroclimate influence is likely unrealistic and points to possible deficiencies in the model.

For CESM and E3SM, switching from the Zender to Kok dust scheme slightly reduces the wind-dominated dust fraction: from 85% to 79% in CESM, and from 99% to 96% in E3SM. The GISS-E2 models yield similar results regardless of model version or aerosol scheme, with 87–90% dust from the wind-dominated regime. Likewise, UKESM1.0 and HadGEM3-GC3.1 yield nearly identical estimates, with 90% of dust from wind-dominated regions. MERRA2 simulates 98% emissions from wind-dominated areas, higher than most ESMs.

The above analysis not only confirms the anomalous dust emission patterns in CanESM5.1 and INM-CM5.0 (shown in Fig. 3), but also identifies GFDL-ESM4 as an outlier due to its misrepresentation of the relative importance of wind and hydroclimate drivers. Here we further examine the wind speed fractional contributions to the total R^2 across different climate zones. For each zone, we use ridgeline plots to illustrate the statistical distributions of grid-level wind-associated R^2 fractions. The results are displayed in Fig. 10. In these plots, the black vertical lines indicate the median values. When the median wind-

associated R^2 fraction is above 50%, more than half of the grid cells within the climate zone are dominated by near-surface winds in the dust variability. Conversely, when the median falls below 50%, hydroclimate drivers exert dominant control over the majority of the climate zone.

In the hyperarid zone (Fig. 10a), most ESMs capture the dominant control of wind speed, with median wind-associated R^2 fractions exceeding 80%. The three GISS-E2 models display similar spatial variability, albeit with slightly lower wind contributions (67–74%). Two models stand out as outliers: GFDL-ESM4 and CESM2-CAM-Kok, both exhibiting great spatial variability and anomalously low wind influence, indicating an overestimation of hydroclimate influence over permanently dry, barren regions. Specifically, GFDL-ESM4 yields a median wind-associated R^2 fraction of 42%, due to excessively strong hydroclimate influence across North Africa, Arabian Peninsula, and Iranian Plateau (see Fig. 8i). Similarly, CESM2-CAM-Kok yields a median of 64%, due to dominant hydroclimate influence over West Africa and the Tarim Basin (see Fig. 8b). In contrast, CESM2-CAM-Zender captures the expected wind dominance with a median of 87%. The overestimated hydroclimate influence in CESM2-CAM-Kok relative to CESM2-CAM-Zender persists even when compared over common dust-emitting areas in the models.

In the arid zone (Fig. 10b), the total R^2 values are generally lower, reflecting reduced explanatory power of the selected predictors. The ESMs also exhibit greater discrepancies in the relative importance of wind and hydroclimate drivers. Although the wind influence is reduced and more variable than in the hyperarid zone, it remains dominant in most ESMs. The GISS-E2 models simulate nearly equal wind and hydroclimate influences. Four models—GFDL-ESM4, INM-CM5.0, MIROC-ES2L and MIROC6—exhibit median wind-associated R^2 fractions well below 50%, signifying a transition from wind- to hydroclimate-dominated regimes. CESM2-CAM-Kok also reflects this transition, although to a small extent with a median of 46%. In both CESM and E3SM, replacing the Zender with Kok dust scheme weakens the wind influence while strengthening the hydroclimate influence, with the median wind-associated R^2 fraction declining from 56% to 44% in CESM and from 86% to 74%. This is consistent with previous findings that physically based soil erodibility formulations in the Kok scheme enhance the dust sensitivity to climate variability Kok et al. (2014a).

Results for the semiarid zone (Fig. 10c) are less robust due to significantly smaller dust-emitting areas or grid cells (see Fig. 1). Overall, the influence of wind speed further weakens, while hydroclimate drivers become more important. The magnitude of this shift, however, varies considerably among ESMs. Specifically, only three models (E3SM3-Kok, EC-Earth3-AerChem and MPI-ESM1.2) retain the wind dominance, albeit with greater spatial variability. Hydroclimate dominance persists in CESM2-CAM-Kok, GFDL-ESM4, INM-CM5.0, MIROC-ES2L and MIROC6, consistent with their behaviors in the arid climate zone. In contrast, multiple models display a transition from wind- to hydroclimate-dominated regimes: E3SM2-Zender, CNRM-ESM2.1, CanESM5.1, HadGEM3-GC3.1, and UKESM1.0. The GISS-E2 models and IPSL-CM6A exhibit moderate increases of hydroclimate influence, resulting in roughly equal importance of wind and hydroclimate drivers. Compared to the ESMs, MERRA2 generally produces dominant wind influence across all three climate zones.

The above analysis indicates that GFDL-ESM4 and CESM2-CAM-Kok simulate anomalously strong hydroclimate influences within the hyperarid zone. To diagnose the sources of these anomalies, Fig. 11 presents the median fractional contributions of five hydroclimate variables to the total R^2. In the hyperarid zone, most ESMs capture the expected negligible influence

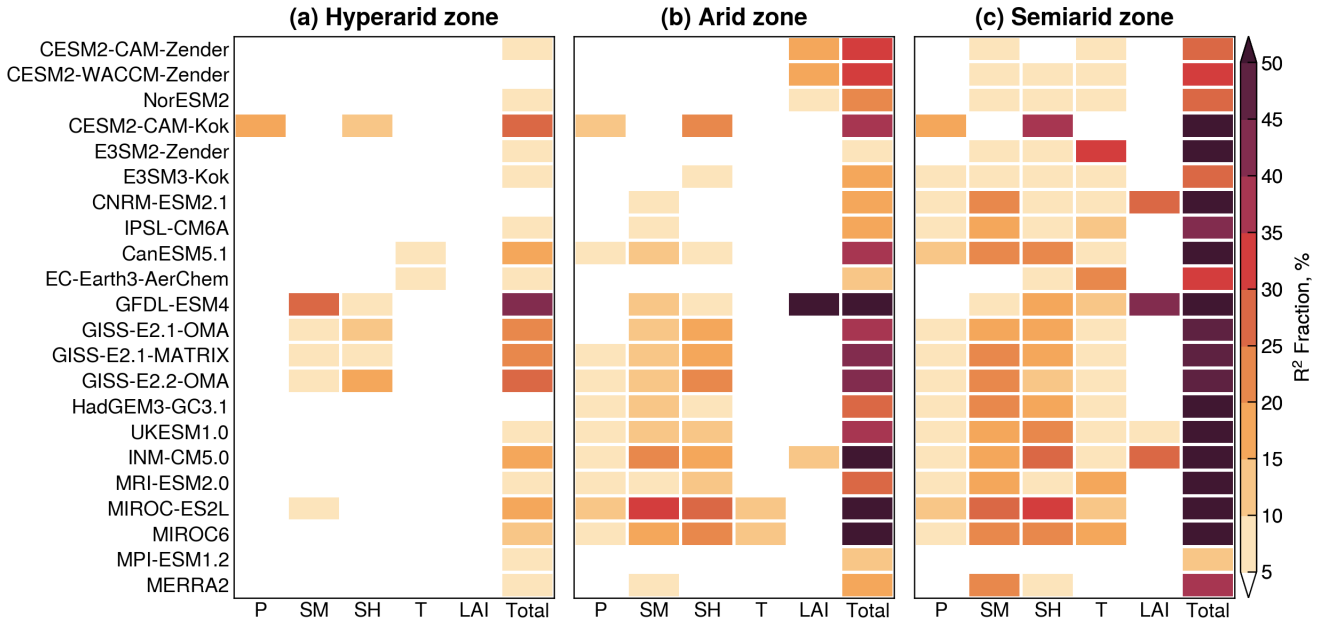

Figure 11. Median factional contributions of hydroclimate drivers to the total explained variance (R^2) in Earth system models and MERRA2 over (a) hyperarid, (b) arid, and (c) semiarid climate zones. Hydroclimate variables are precipitation (P), soil moisture (SM), specific humidity (SH), air temperature (T), and leaf area index (LAI).

of hydroclimate drivers. GFDL-ESM4 and CESM2-CAM-Kok stand out as outliers, producing anomalously high influence from soil moisture and precipitation, respectively. The influence attributed to specific humidity can be interpreted as a soil moisture effect, given the close coupling between surface soil water content and near-surface humidity through evapotranspiration. The GISS-E2 models also display elevated contributions from soil moisture and specific humidity, which explains their modest wind influence in the hyperarid zone, as shown in Fig. 10a.

The anomalous hydroclimate influence in the hyperarid zone can be explained by two possible mechanisms: (1) the model overestimates the hydroclimate variability, leading to spurious effects on dust emissions; or (2) the model reasonably represents the hydroclimate variability but overestimates the dust sensitivity to hydroclimate drivers. For example, Shevliakova et al. (2024) reported that the GFDL-ESM4 land model significantly overestimates surface soil moisture over major dust source areas, by as much as a factor of two compared to satellite observations. This bias likely explains the unrealistically large soil moisture influence on dust emissions in GFDL-ESM4.

The anomalous hydroclimate influence in CESM2-CAM-Kok may be partly due to dust emission parameterizations in the Kok scheme which introduces enhanced sensitivity to soil moisture compared with the Zender scheme (Kok et al., 2014a). Another possible reason is the short simulation period for CESM2-CAM-Kok (2004–2013), which may be insufficient to capture the full range of dust variability and predictor relationships relative to CESM2-CAM-Zender (1980–2014). In this regard, the E3SM experiments provide a more robust comparison between the two dust schemes. As shown in Fig. 11a, both

E3SM2-Zender and E3SM3-Kok exhibit negligible hydroclimate influence in the hyperarid zone. In the arid zone, however, E3SM3-Kok exhibits stronger hydroclimate influence than E3SM2-Zender, providing new evidence that the Kok scheme amplifies the dust emission sensitivity to hydroclimate conditions compared to the Zender scheme, as previously suggested by Kok et al. (2014a).

In the arid zone (Fig. 11b), the enhanced hydroclimate influence is primarily attributed to soil moisture and specific humidity in most ESMs, consistent with their well-established role in modulating soil erodibility (e.g., Csavina et al., 2014; RAVI et al., 2006; Kim and Choi, 2015). Several models—including CESM, GFDL-ESM4 and INM-CM5.0—assign strong influence to LAI. Unlike other hydroclimate variables, LAI may be either prescribed from climatology or interactively simulated in models coupled with dynamic vegetation components, such as CESM and GFDL-ESM4 (Table 1). Models using prescribed LAI are likely to show limited interannual variability and minimal influence on dust emissions. For CESM and GFDL-ESM4, the LAI influence reflects the vegetation effect on bare soil fraction, a key parameter in vertical dust flux calculations. Specifically, bare soil fraction is calculated from LAI assuming a linear relationship in CESM and an exponential relationship in GFDL-ESM4.

4 Conclusions

This study evaluates discrepancies among 21 ESMs in representing the interannual variability of windblown dust emissions and the relative importance of near-surface wind speed and five hydroclimate variables (precipitation, soil moisture, specific humidity, air temperature, and LAI) in modulating the dust variability. Treating dust emission flux as an unobservable, model-specific quantity, we apply dominance analysis to quantify the relative influences of physical drivers within each model, and compare the model behaviors across three climatologically-defined climate zones (hyperarid, arid, and semiarid).

The extent of inter-model agreement in simulated dust variability exhibits a strong dependence on climate aridity. In the hyperarid zone, the ESMs show poor agreement, with only 10% out of 210 pairwise comparisons yielding statistically significant, positive correlations. This poor agreement largely reflects inconsistencies in simulated near-surface winds. In arid and semiarid zones, the ESMs exhibit a dual pattern driven by a "double-edged sword" effect of land surface memory: models with coherent representations of hydroclimate variability tend to converge in their simulated dust variability, whereas those with divergent hydroclimate representations diverge in dust emission responses.

The relative importance of wind and hydroclimate drivers also varies with climate aridity. In the hyperarid zone, most ESMs capture the expected dominant wind control and minimal hydroclimate influence, except CESM2-CAM-Kok and GFDL-ESM4, which show unusually strong sensitivities to precipitation and soil moisture. The overestimated hydroclimate influence in GFDL-ESM4 can be explained by the model's overestimation of soil moisture in drylands and consequent spurious effects on dust emissions. The overestimated hydroclimate influence in CESM2-CAM-Kok may be partly explained by the physically based soil erodibility formulation in the Kok et al. (2014b) dust scheme. A similar pattern is found in E3SM, where replacing the Zender et al. (2003) scheme with the Kok et al. (2014b) scheme enhances the hydroclimate contribution to dust variability in the arid zone. Due to compounding factors such as model physics and dust mineralogy treatments in CESM and E3SM,

however, additional experiments are needed to disentangle the effects of dust emission parameterizations on the simulated sensitivities to physical drivers.

In arid and semiarid zones, the wind influence generally weakens while the hydroclimate influence strengthens in all ESMs. But the relative importance of these drivers becomes increasingly inconsistent, with contrasting model behaviors in either retaining wind dominance or shifting toward hydroclimate dominance or near-equal importance between the two. Compared to the ESMs, MERRA2 generally produce stronger wind influence and weaker hydroclimate influence across all three climate zones.

Overall, this study provides new insights into how current ESMs represent the interannual variability and physical drivers of windblown dust emissions. Our findings underscore that reducing model uncertainties in dust emission simulations requires (1) improved representations of near-surface wind variability and gustiness in hyperarid regions, and (2) more accurate treatment of hydroclimate and land-surface processes in arid and semiarid regions.

Data availability. Model comparison and dominance analysis results are available at https://doi.org/10.5281/zenodo.15741734.

Author contributions. XX designed this study with input from LL. XX and XL performed the analysis and wrote the initial manuscript. LL performed CESM2-CAM-Kok simulations. YF performed E3SM simulations. All authors edited the manuscript.

Competing interests. The authors declare no competing interests.

Acknowledgements. X.L. and X.X. are partially supported by the NASA Land-Cover and Land-Use Change Program. Y.F. acknowledges the support of the Energy Exascale Earth System Model (E3SM) project, funded by the U.S. Department of Energy (DOE), Office of Science, Office of Biological and Environmental Research. The work at Argonne National Laboratory was supported by the U.S. DOE Office of Science under contract DE-AC02-06CH11357. L.L. acknowledges support from the U.S. Department of Energy (DOE) under award DE-SC0021302, and from the Earth Surface Mineral Dust Source Investigation (EMIT), a National Aeronautics and Space Administration (NASA) Earth Ventures-Instrument (EVI-4) mission. He also acknowledges the high-performance computing resources provided by Derecho at the National Center for Atmospheric Research (NCAR), through NCAR's Computational and Information Systems Laboratory (CISL), which is sponsored by the National Science Foundation (NSF). The authors acknowledge the World Climate Research Programme for coordinating and promoting CMIP6, and thank the climate modeling groups for producing and making available their model output, the Earth System Grid Federation (ESGF) for archiving the data and providing access, and the multiple funding agencies who support CMIP6 and ESGF.

References

Albani, S., Mahowald, N. M., Perry, A. T., Scanza, R. A., Zender, C. S., Heavens, N. G., Maggi, V., Kok, J. F., and Otto-Bliesner, B. L.: Improved dust representation in the Community Atmosphere Model, Journal of Advances in Modeling Earth Systems, 6, 541–570, https://doi.org/10.1002/2013MS000279, 2015.

Aryal, Y. N. and Evans, S.: Global Dust Variability Explained by Drought Sensitivity in CMIP6 Models, Journal of Geophysical Research: Earth Surface, 126, https://doi.org/10.1029/2021JF006073, 2021.

Azen, R. and Budescu, D. V.: The Dominance Analysis Approach for Comparing Predictors in Multiple Regression, Psychological Methods, 8, 129–148, https://doi.org/10.1037/1082-989X.8.2.129, 2003.

Balkanski, Y., Schulz, M., Claquin, T., Moulin, C., and Ginoux, P.: Global Emissions of Mineral Aerosol: Formulation and Validation using Satellite Imagery, in: Emissions of Atmospheric Trace Compounds, edited by Granier, C., Artaxo, P., and Reeves, C. E., pp. 239–267, Springer, https://doi.org/10.1007/978-1-4020-2167-1_6, 2004.

Bauer, S. E., Tsigaridis, K., Faluvegi, G., Nazarenko, L., Miller, R. L., Kelley, M., and Schmidt, G.: The Turning Point of the Aerosol Era, Journal of Advances in Modeling Earth Systems, 14, https://doi.org/10.1029/2022MS003070, 2022.

Bryant, R. G.: Recent advances in our understanding of dust source emission processes, Progress in Physical Geography, 37, 397–421, https://doi.org/10.1177/0309133313479391, 2013.

Budescu, D. V.: Dominance analysis: A new approach to the problem of relative importance of predictors in multiple regression, Psychological Bulletin, 114, 542–551, https://doi.org/10.1037/0033-2909.114.3.542, 1993.

Bullard, J. E., Harrison, S. P., Baddock, M. C., Drake, N., Gill, T. E., McTainsh, G., and Sun, Y.: Preferential dust sources: A geomorphological classification designed for use in global dust-cycle models, Journal of Geophysical Research: Earth Surface, 116, https://doi.org/10.1029/2011JF002061, 2011.

Cheng, T., Peng, Y., Feichter, J., and Tegen, I.: An improvement on the dust emission scheme in the global aerosol-climate model ECHAM5-HAM, Atmospheric Chemistry and Physics, 8, 1105–1117, https://doi.org/10.5194/acp-8-1105-2008, 2008.

Cowie, S. M., Marsham, J. H., and Knippertz, P.: The importance of rare, high-wind events for dust uplift in northern Africa, Geophysical Research Letters, 42, 8208–8215, https://doi.org/10.1002/2015GL065819, 2015.

Csavina, J., Field, J., Félix, O., Corral-Avitia, A. Y., Sáez, A. E., and Betterton, E. A.: Effect of wind speed and relative humidity on atmospheric dust concentrations in semi-arid climates, Science of the Total Environment, 487, 82–90, https://doi.org/10.1016/j.scitotenv.2014.03.138, 2014.

Engelstaedter, S., Kohfeld, K. E., Tegen, I., and Harrison, S. P.: Controls of dust emissions by vegetation and topographic depressions: An evaluation using dust storm frequency data, Geophysical Research Letters, 30, https://doi.org/10.1029/2002GL016471, 2003.

Evan, A. T.: Surface Winds and Dust Biases in Climate Models, Geophysical Research Letters, 45, 1079–1085, https://doi.org/10.1002/2017GL076353, 2018.

Evan, A. T., Flamant, C., Fiedler, S., and Doherty, O.: An analysis of aeolian dust in climate models, Geophysical Research Letters, 41, 5996–6001, https://doi.org/10.1002/2014GL060545, 2014.

Evans, S., Ginoux, P., Malyshev, S., and Shevliakova, E.: Climate-vegetation interaction and amplification of Australian dust variability, Geophysical Research Letters, 43, 823–11, https://doi.org/10.1002/2016GL071016, 2016.

Fécan, F., Marticorena, B., and Bergametti, G.: Parametrization of the increase of the aeolian erosion threshold wind friction velocity due to soil moisture for arid and semi-arid areas, Annales Geophysicae, 17, 149, https://doi.org/10.1007/s005850050744, 1999.

Feng, Y., Wang, H., Rasch, P. J., Zhang, K., Lin, W., Tang, Q., Xie, S., Hamilton, D. S., Mahowald, N., and Yu, H.: Global Dust Cycle and Direct Radiative Effect in E3SM Version 1: Impact of Increasing Model Resolution, Journal of Advances in Modeling Earth Systems, https://doi.org/10.1029/2021MS002909, 2022.

Gelaro, R., McCarty, W., Suárez, M. J., Todling, R., Molod, A., Takacs, L., Randles, C. A., Darmenov, A., Bosilovich, M. G., Reichle, R., Wargan, K., Coy, L., Cullather, R., Draper, C., Akella, S., Buchard, V., Conaty, A., da Silva, A. M., Gu, W., Kim, G. K., Koster, R., Lucchesi, R., Merkova, D., Nielsen, J. E., Partyka, G., Pawson, S., Putman, W., Rienecker, M., Schubert, S. D., Sienkiewicz, M., and Zhao, B.: The modern-era retrospective analysis for research and applications, version 2 (MERRA-2), Journal of Climate, 30, 5419–5454, https://doi.org/10.1175/JCLI-D-16-0758.1, 2017.

Gettelman, A., Mills, M. J., Kinnison, D. E., Garcia, R. R., Smith, A. K., Marsh, D. R., Tilmes, S., Vitt, F., Bardeen, C. G., McInerny, J., Liu, H. L., Solomon, S. C., Polvani, L. M., Emmons, L. K., Lamarque, J. F., Richter, J. H., Glanville, A. S., Bacmeister, J. T., Phillips, A. S., Neale, R. B., Simpson, I. R., DuVivier, A. K., Hodzic, A., and Randel, W. J.: The Whole Atmosphere Community Climate Model Version 6 (WACCM6), Journal of Geophysical Research: Atmospheres, 124, 12 380–12 403, https://doi.org/10.1029/2019JD030943, 2019.

Ginoux, P., Chin, M., Tegen, I., Prospero, J. M., Holben, B., Dubovik, O., and Lin, S. J.: Sources and distributions of dust aerosols simulated with the GOCART model, Journal of Geophysical Research Atmospheres, 106, 20 255–20 273, https://doi.org/10.1029/2000JD000053, 2001.

Ginoux, P., Prospero, J. M., Gill, T. E., Hsu, N. C., and Zhao, M.: Global-scale attribution of anthropogenic and natural dust sources and their emission rates based on MODIS Deep Blue aerosol products, Reviews of Geophysics, 50, https://doi.org/10.1029/2012RG000388, 2012.

Gliß, J., Mortier, A., Schulz, M., Andrews, E., Balkanski, Y., Bauer, S. E., Benedictow, A. M., Bian, H., Checa-Garcia, R., Chin, M., Ginoux, P., Griesfeller, J. J., Heckel, A., Kipling, Z., Kirkeväg, A., Kokkola, H., Laj, P., Le Sager, P., Tronstad Lund, M., Lund Myhre, C., Matsui, H., Myhre, G., Neubauer, D., Van Noije, T., North, P., Olivié, D. J., Rémy, S., Sogacheva, L., Takemura, T., Tsigaridis, K., and Tsyro, S. G.: AeroCom phase III multi-model evaluation of the aerosol life cycle and optical properties using ground- And space-based remote sensing as well as surface in situ observations, Atmospheric Chemistry and Physics, 21, 87–128, https://doi.org/10.5194/acp-21-87-2021, 2021.

Hajima, T., Watanabe, M., Yamamoto, A., Tatebe, H., Noguchi, M. A., Abe, M., Ohgaito, R., Ito, A., Yamazaki, D., Okajima, H., Ito, A., Takata, K., Ogochi, K., Watanabe, S., and Kawamiya, M.: Development of the MIROC-ES2L Earth system model and the evaluation of biogeochemical processes and feedbacks, Geoscientific Model Development, 13, 2197–2244, https://doi.org/10.5194/gmd-13-2197-2020, 2020.

Huneeus, N., Schulz, M., Balkanski, Y., Griesfeller, J., Prospero, J., Kinne, S., Bauer, S., Boucher, O., Chin, M., Dentener, F., Diehl, T., Easter, R., Fillmore, D., Ghan, S., Ginoux, P., Grini, A., Horowitz, L., Koch, D., Krol, M. C., Landing, W., Liu, X., Mahowald, N., Miller, R., Morcrette, J. J., Myhre, G., Penner, J., Perlwitz, J., Stier, P., Takemura, T., and Zender, C. S.: Global dust model intercomparison in AeroCom phase i, Atmospheric Chemistry and Physics, 11, 7781–7816, https://doi.org/10.5194/acp-11-7781-2011, 2011.

Kim, D., Chin, M., Yu, H., Diehl, T., Tan, Q., Kahn, R. A., Tsigaridis, K., Bauer, S. E., Takemura, T., Pozzoli, L., Bellouin, N., Schulz, M., Peyridieu, S., Chédin, A., and Koffi, B.: Sources, sinks, and transatlantic transport of North African dust aerosol: A multimodel analysis and comparison with remote sensing data, Journal of Geophysical Research, 119, 6259–6277, https://doi.org/10.1002/2013JD021099, 2014.

Kim, D., Chin, M., Schuster, G., Yu, H., Takemura, T., Tuccella, P., Ginoux, P., Liu, X., Shi, Y., Matsui, H., Tsigaridis, K., Bauer, S. E., Kok, J. F., and Schulz, M.: Where Dust Comes From: Global Assessment of Dust Source Attributions With AeroCom Models, Journal of Geophysical Research: Atmospheres, 129, e2024JD041 377, https://doi.org/https://doi.org/10.1029/2024JD041377, 2024.

Kim, H. and Choi, M.: Impact of soil moisture on dust outbreaks in East Asia: Using satellite and assimilation data, Geophysical Research Letters, 42, 2789–2796, https://doi.org/https://doi.org/10.1002/2015GL063325, 2015.

Knippertz, P. and Todd, M. C.: Mineral dust aerosols over the Sahara: Meteorological controls on emission and transport and implications for modeling, Reviews of Geophysics, 50, https://doi.org/10.1029/2011RG000362, 2012.

Kok, J. F., Albani, S., Mahowald, N. M., and Ward, D. S.: An improved dust emission model - Part 2: Evaluation in the Community Earth System Model, with implications for the use of dust source functions, Atmospheric Chemistry and Physics, 14, 13 043–13 061, https://doi.org/10.5194/acp-14-13043-2014, 2014a.

Kok, J. F., Mahowald, N. M., Fratini, G., Gillies, J. A., Ishizuka, M., Leys, J. F., Mikami, M., Park, M. S., Park, S. U., Van Pelt, R. S., and Zobeck, T. M.: An improved dust emission model - Part 1: Model description and comparison against measurements, Atmospheric Chemistry and Physics, 14, 13 023–13 041, https://doi.org/10.5194/acp-14-13023-2014, 2014b.

Kok, J. F., Storelvmo, T., Karydis, V. A., Adebiyi, A. A., Mahowald, N. M., Evan, A. T., He, C., and Leung, D. M.: Mineral dust aerosol impacts on global climate and climate change, Nature Reviews Earth and Environment, 4, 71–86, https://doi.org/10.1038/s43017-022-00379-5, 2023.

Koster, R. D., Guo, Z., Yang, R., Dirmeyer, P. A., Mitchell, K., and Puma, M. J.: On the nature of soil moisture in land surface models, Journal of Climate, 22, 4322–4335, https://doi.org/10.1175/2009JCLI2832.1, 2009.

Li, L., Mahowald, N. M., Kok, J. F., Liu, X., Wu, M., Leung, D. M., Hamilton, D. S., Emmons, L. K., Huang, Y., Sexton, N., Meng, J., and Wan, J.: Importance of different parameterization changes for the updated dust cycle modeling in the Community Atmosphere Model (version 6.1), Geoscientific Model Development, 15, 8181–8219, https://doi.org/10.5194/gmd-15-8181-2022, 2022.

Li, L., Mahowald, N. M., Gonçalves Ageitos, M., Obiso, V., Miller, R. L., Pérez García-Pando, C., Di Biagio, C., Formenti, P., Brodrick, P. G., Clark, R. N., Green, R. O., Kokaly, R., Swayze, G., and Thompson, D. R.: Improved constraints on hematite refractive index for estimating climatic effects of dust aerosols, Communications Earth & Environment, 5, 295, https://doi.org/10.1038/s43247-024-01441-4, 2024.

Lurton, T., Balkanski, Y., Bastrikov, V., Bekki, S., Bopp, L., Braconnot, P., Brockmann, P., Cadule, P., Contoux, C., Cozic, A., Cugnet, D., Dufresne, J.-L., Éthé, C., Foujols, M.-A., Ghattas, J., Hauglustaine, D., Hu, R.-M., Kageyama, M., Khodri, M., Lebas, N., Levavasseur, G., Marchand, M., Ottlé, C., Peylin, P., Sima, A., Szopa, S., Thiéblemont, R., Vuichard, N., and Boucher, O.: Implementation of the CMIP6 Forcing Data in the IPSL-CM6A-LR Model, Journal of Advances in Modeling Earth Systems, 12, e2019MS001 940, https://doi.org/https://doi.org/10.1029/2019MS001940, 2020.

Marticorena, B. and Bergametti, G.: Modeling the atmospheric dust cycle: 1. Design of a soil-derived dust emission scheme, Journal of Geophysical Research, 100, https://doi.org/10.1029/95jd00690, 1995.

Mauritsen, T., Bader, J., Becker, T., Behrens, J., Bittner, M., Brokopf, R., Brovkin, V., Claussen, M., Crueger, T., Esch, M., Fast, I., Fiedler, S., Fläschner, D., Gayler, V., Giorgetta, M., Goll, D. S., Haak, H., Hagemann, S., Hedemann, C., Hohenegger, C., Ilyina, T., Jahns, T., Jimenéz-de-la Cuesta, D., Jungclaus, J., Kleinen, T., Kloster, S., Kracher, D., Kinne, S., Kleberg, D., Lasslop, G., Kornblueh, L., Marotzke, J., Matei, D., Meraner, K., Mikolajewicz, U., Modali, K., Möbis, B., Müller, W. A., Nabel, J. E. M. S., Nam, C. C. W., Notz, D., Nyawira, S.-S., Paulsen, H., Peters, K., Pincus, R., Pohlmann, H., Pongratz, J., Popp, M., Raddatz, T. J., Rast, S., Redler, R., Reick, C. H., Rohrschneider, T., Schemann, V., Schmidt, H., Schnur, R., Schulzweida, U., Six, K. D., Stein, L., Stemmler, I., Stevens, B., von Storch, J.-S., Tian, F., Voigt, A., Vrese, P., Wieners, K.-H., Wilkenskjeld, S., Winkler, A., and Roeckner, E.: Developments in the MPI-M Earth System Model version 1.2 (MPI-ESM1.2) and Its Response to Increasing CO2, Journal of Advances in Modeling Earth Systems, 11, 998–1038, https://doi.org/https://doi.org/10.1029/2018MS001400, 2019.

Miller, R. L., Cakmur, R. V., Perlwitz, J., Geogdzhayev, I. V., Ginoux, P., Koch, D., Kohfeld, K. E., Prigent, C., Ruedy, R., Schmidt, G. A., and Tegen, I.: Mineral dust aerosols in the NASA Goddard Institute for Space Sciences ModelE atmospheric general circulation model, Journal of Geophysical Research Atmospheres, 111, https://doi.org/10.1029/2005JD005796, 2006.

Miller, R. L., Schmidt, G. A., Nazarenko, L. S., Bauer, S. E., Kelley, M., Ruedy, R., Russell, G. L., Ackerman, A. S., Aleinov, I., Bauer, M., Bleck, R., Canuto, V., Cesana, G., Cheng, Y., Clune, T. L., Cook, B. I., Cruz, C. A., Del Genio, A. D., Elsaesser, G. S., Faluvegi, G., Kiang, N. Y., Kim, D., Lacis, A. A., Leboissetier, A., LeGrande, A. N., Lo, K. K., Marshall, J., Matthews, E. E., McDermid, S., Mezuman, K., Murray, L. T., Oinas, V., Orbe, C., Pérez García-Pando, C., Perlwitz, J. P., Puma, M. J., Rind, D., Romanou, A., Shindell, D. T., Sun, S., Tausnev, N., Tsigaridis, K., Tselioudis, G., Weng, E., Wu, J., and Yao, M. S.: CMIP6 Historical Simulations (1850–2014) With GISS-E2.1, Journal of Advances in Modeling Earth Systems, 13, https://doi.org/10.1029/2019MS002034, 2021.

Nandintsetseg, B. and Shinoda, M.: Land surface memory effects on dust emission in a Mongolian temperate grassland, Journal of Geophysical Research: Biogeosciences, 120, 414–427, https://doi.org/10.1002/2014JG002708, 2015.

Peng, Y., Von Salzen, K., and Li, J.: Simulation of mineral dust aerosol with Piecewise Log-normal Approximation (PLA) in CanAM4-PAM, Atmospheric Chemistry and Physics, 12, 6891–6914, https://doi.org/10.5194/acp-12-6891-2012, 2012.

Prospero, J. M. and Lamb, P. J.: African Droughts and Dust Transport to the Caribbean: Climate Change Implications, Science, 302, 1024–1027, https://doi.org/10.1126/science.1089915, 2003.

Prospero, J. M., Ginoux, P., Torres, O., Nicholson, S. E., and Gill, T. E.: Environmental characterization of global sources of atmospheric soil dust identified with the Nimbus 7 Total Ozone Mapping Spectrometer (TOMS) absorbing aerosol product, Reviews of Geophysics, 40, 2–1, https://doi.org/10.1029/2000RG000095, 2002.

Pu, B. and Ginoux, P.: The impact of the Pacific Decadal Oscillation on springtime dust activity in Syria, Atmospheric Chemistry and Physics, 16, 13 431–13 448, https://doi.org/10.5194/acp-16-13431-2016, 2016.

Pu, B. and Ginoux, P.: How reliable are CMIP5 models in simulating dust optical depth?, Atmospheric Chemistry and Physics, 18, 12 491–12 510, https://doi.org/10.5194/acp-18-12491-2018, 2018.

Randles, C. A., da Silva, A. M., Buchard, V., Colarco, P. R., Darmenov, A., Govindaraju, R., Smirnov, A., Holben, B., Ferrare, R., Hair, J., Shinozuka, Y., and Flynn, C. J.: The MERRA-2 aerosol reanalysis, 1980 onward. Part I: System description and data assimilation evaluation, Journal of Climate, 30, 6823–6850, https://doi.org/10.1175/JCLI-D-16-0609.1, 2017.

RAVI, S., ZOBECK, T. E. D. M., OVER, T. M., OKIN, G. S., and D'ODORICO, P.: On the effect of moisture bonding forces in air-dry soils on threshold friction velocity of wind erosion, Sedimentology, 53, 597–609, https://doi.org/https://doi.org/10.1111/j.1365-3091.2006.00775.x, 2006.

Rind, D., Orbe, C., Jonas, J., Nazarenko, L., Zhou, T., Kelley, M., Lacis, A., Shindell, D., Faluvegi, G., Romanou, A., Russell, G., Tausnev, N., Bauer, M., and Schmidt, G.: GISS Model E2.2: A Climate Model Optimized for the Middle Atmosphere—Model Structure, Climatology, Variability, and Climate Sensitivity, Journal of Geophysical Research: Atmospheres, 125, https://doi.org/10.1029/2019JD032204, 2020.

Roberts, M. J., Baker, A., Blockley, E. W., Calvert, D., Coward, A., Hewitt, H. T., Jackson, L. C., Kuhlbrodt, T., Mathiot, P., Roberts, C. D., Schiemann, R., Seddon, J., Vannière, B., and Vidale, P. L.: Description of the resolution hierarchy of the global coupled HadGEM3-GC3.1 model as used in CMIP6 HighResMIP experiments, Geosci. Model Dev., 12, 4999–5028, https://doi.org/10.5194/gmd-12-4999-2019, 2019.

Séférian, R., Nabat, P., Michou, M., Saint-Martin, D., Voldoire, A., Colin, J., Decharme, B., Delire, C., Berthet, S., Chevallier, M., Sénési, S., Franchisteguy, L., Vial, J., Mallet, M., Joetzjer, E., Geoffroy, O., Guérémy, J. F., Moine, M. P., Msadek, R., Ribes, A., Rocher, M., Roehrig, R., Salas-y Mélia, D., Sanchez, E., Terray, L., Valcke, S., Waldman, R., Aumont, O., Bopp, L., Deshayes, J., Éthé, C., and Madec, G.:

Evaluation of CNRM Earth System Model, CNRM-ESM2-1: Role of Earth System Processes in Present-Day and Future Climate, Journal of Advances in Modeling Earth Systems, 11, 4182–4227, https://doi.org/10.1029/2019MS001791, 2019.

Seland, O., Bentsen, M., Olivié, D., Toniazzo, T., Gjermundsen, A., Graff, L. S., Debernard, J. B., Gupta, A. K., He, Y. C., Kirkeväg, A., Schwinger, J., Tjiputra, J., Schanke Aas, K., Bethke, I., Fan, Y., Griesfeller, J., Grini, A., Guo, C., Ilicak, M., Karset, I. H. H., Landgren, O., Liakka, J., Moseid, K. O., Nummelin, A., Spensberger, C., Tang, H., Zhang, Z., Heinze, C., Iversen, T., and Schulz, M.: Overview of the Norwegian Earth System Model (NorESM2) and key climate response of CMIP6 DECK, historical, and scenario simulations, Geoscientific Model Development, 13, 6165–6200, https://doi.org/10.5194/gmd-13-6165-2020, 2020.

Shao, Y., Raupach, M. R., and Leys, J. F.: A model for predicting aeolian sand drift and dust entrainment on scales from paddock to region, Australian Journal of Soil Research, 34, 309–342, https://doi.org/10.1071/SR9960309, 1996.

Shao, Y., Wyrwoll, K. H., Chappell, A., Huang, J., Lin, Z., McTainsh, G. H., Mikami, M., Tanaka, T. Y., Wang, X., and Yoon, S.: Dust cycle: An emerging core theme in Earth system science, Aeolian Research, 2, 181–204, https://doi.org/10.1016/j.aeolia.2011.02.001, 2011.

Shevliakova, E., Malyshev, S., Martinez-Cano, I., Milly, P. C. D., Pacala, S. W., Ginoux, P., Dunne, K. A., Dunne, J. P., Dupuis, C., Findell, K. L., Ghannam, K., Horowitz, L. W., Knutson, T. R., Krasting, J. P., Naik, V., Phillipps, P., Zadeh, N., Yu, Y., Zeng, F., and Zeng, Y.: The Land Component LM4.1 of the GFDL Earth System Model ESM4.1: Model Description and Characteristics of Land Surface Climate and Carbon Cycling in the Historical Simulation, Journal of Advances in Modeling Earth Systems, 16, e2023MS003 922, https://doi.org/https://doi.org/10.1029/2023MS003922, 2024.

Shinoda, M., Gillies, J. A., Mikami, M., and Shao, Y.: Temperate grasslands as a dust source: Knowledge, uncertainties, and challenges, Aeolian Research, 3, 271–293, https://doi.org/10.1016/j.aeolia.2011.07.001, 2011.

Sigmond, M., Anstey, J., Arora, V., Digby, R., Gillett, N., Kharin, V., Merryfield, W., Reader, C., Scinocca, J., Swart, N., Virgin, J., Abraham, C., Cole, J., Lambert, N., Lee, W. S., Liang, Y., Malinina, E., Rieger, L., Von Salzen, K., Seiler, C., Seinen, C., Shao, A., Sospedra-Alfonso, R., Wang, L., and Yang, D.: Improvements in the Canadian Earth System Model (CanESM) through systematic model analysis: CanESM5.0 and CanESM5.1, Geoscientific Model Development, 16, 6553–6591, https://doi.org/10.5194/gmd-16-6553-2023, 2023.

Sokolik, I. N., Darmenova, K., Huang, J., Kalashnikova, O., Kurosaki, Y., and Xi, X.: Examining changes in land cover and land use, regional climate and dust in Dryland East Asia and Their Linkages within the Earth System, in: Dryland East Asia: Land Dynamics amid Social and Climate Change, edited by Chen, J., Wan, S., Henebry, G., Qi, J., Gutman, G., Sun, G., and Kappas, M., chap. 9, pp. 183–211, DE GRUYTER, Berlin, Boston, ISBN 9783110287912, https://doi.org/10.1515/9783110287912.183, 2021.

Takemura, T., Egashira, M., Matsuzawa, K., Ichijo, H., O'Ishi, R., and Abe-Ouchi, A.: A simulation of the global distribution and radiative forcing of soil dust aerosols at the Last Glacial Maximum, Atmospheric Chemistry and Physics, 9, 3061–3073, https://doi.org/10.5194/acp-9-3061-2009, 2009.

Tatebe, H., Ogura, T., Nitta, T., Komuro, Y., Ogochi, K., Takemura, T., Sudo, K., Sekiguchi, M., Abe, M., Saito, F., Chikira, M., Watanabe, S., Mori, M., Hirota, N., Kawatani, Y., Mochizuki, T., Yoshimura, K., Takata, K., O'Ishi, R., Yamazaki, D., Suzuki, T., Kurogi, M., Kataoka, T., Watanabe, M., and Kimoto, M.: Description and basic evaluation of simulated mean state, internal variability, and climate sensitivity in MIROC6, Geoscientific Model Development, 12, 2727–2765, https://doi.org/10.5194/gmd-12-2727-2019, 2019.

Tegen, I., Harrison, S. P., Kohfeld, K., Prentice, I. C., Coe, M., and Heimann, M.: Impact of vegetation and preferential source areas on global dust aerosol: Results from a model study, Journal of Geophysical Research Atmospheres, 107, https://doi.org/10.1029/2001JD000963, 2002.

Tegen, I., Neubauer, D., Ferrachat, S., Drian, C. S. L., Bey, I., Schutgens, N., Stier, P., Watson-Parris, D., Stanelle, T., Schmidt, H., Rast, S., Kokkola, H., Schultz, M., Schroeder, S., Daskalakis, N., Barthel, S., Heinold, B., and Lohmann, U.: The global aerosol-climate model

echam6.3-ham2.3 -Part 1: Aerosol evaluation, Geoscientific Model Development, 12, 1643–1677, https://doi.org/10.5194/gmd-12-1643-2019, 2019.

Textor, C., Schulz, M., Guibert, S., Kinne, S., Balkanski, Y., Bauer, S., Berntsen, T., Berglen, T., Boucher, O., Chin, M., Dentener, F., Diehl, T., Easter, R., Feichter, H., Fillmore, D., Ghan, S., Ginoux, P., Gong, S., Grini, A., Hendricks, J., Horowitz, L., Huang, P., Isaksen, I., Iversen, T., Kloster, S., Koch, D., Kirkevåg, A., Kristjansson, J. E., Krol, M., Lauer, A., Lamarque, J. F., Liu, X., Montanaro, V., Myhre, G., Penner, J., Pitari, G., Reddy, S., Seland, Stier, P., Takemura, T., and Tie, X.: Analysis and quantification of the diversities of aerosol life cycles within AeroCom, Atmospheric Chemistry and Physics, 6, 1777–1813, https://doi.org/10.5194/acp-6-1777-2006, 2006.

Van Noije, T., Bergman, T., Le Sager, P., O'Donnell, D., Makkonen, R., Gonçalves-Ageitos, M., Döscher, R., Fladrich, U., Von Hardenberg, J., Keskinen, J. P., Korhonen, H., Laakso, A., Myriokefalitakis, S., Ollinaho, P., Pérez Garciá-Pando, C., Reerink, T., Schrödner, R., Wyser, K., and Yang, S.: EC-Earth3-AerChem: A global climate model with interactive aerosols and atmospheric chemistry participating in CMIP6, Geoscientific Model Development, 14, 5637–5668, https://doi.org/10.5194/gmd-14-5637-2021, 2021.

Volodin, E. M.: Possible Climate Change in Russia in the 21st Century Based on the INM-CM5-0 Climate Model, Russian Meteorology and Hydrology, 47, 327–333, https://doi.org/10.3103/S1068373922050016, 2022.

Volodin, E. M. and Kostrykin, S. V.: The aerosol module in the INM RAS climate model, Russian Meteorology and Hydrology, 41, 519–528, https://doi.org/10.3103/S106837391608001X, 2016.

Woodward, S.: Modeling the atmospheric life cycle and radiative impact of mineral dust in the Hadley Centre climate model, Journal of Geophysical Research Atmospheres, 106, 18 155–18 166, https://doi.org/10.1029/2000JD900795, 2001.

Woodward, S.: Hadley Centre Technical Note 87 - Mineral dust in HadGEM2, Tech. rep., Met Office, Exeter, 2011.

Woodward, S., Sellar, A. A., Tang, Y., Stringer, M., Yool, A., Robertson, E., and Wiltshire, A.: The simulation of mineral dust in the United Kingdom Earth System Model UKESM1, Atmospheric Chemistry and Physics, 22, 14 503–14 528, https://doi.org/10.5194/acp-22-14503-2022, 2022.

Wu, C., Lin, Z., and Liu, X.: The global dust cycle and uncertainty in CMIP5 (Coupled Model Intercomparison Project phase 5) models, Atmospheric Chemistry and Physics, 20, 10 401–10 425, https://doi.org/10.5194/acp-20-10401-2020, 2020.

Xi, X.: On the Geomorphic, Meteorological, and Hydroclimatic Drivers of the Unusual 2018 Early Summer Salt Dust Storms in Central Asia, Journal of Geophysical Research: Atmospheres, 128, https://doi.org/10.1029/2022JD038089, 2023.

Xi, X. and Sokolik, I. N.: Seasonal dynamics of threshold friction velocity and dust emission in Central Asia, Journal of Geophysical Research: Atmospheres, 120, 1536–1564, https://doi.org/10.1002/2014JD022471, 2015a.

Xi, X. and Sokolik, I. N.: Dust interannual variability and trend in Central Asia from 2000 to 2014 and their climatic linkages, Journal of Geophysical Research: Atmospheres, 120, 12 175–12 197, https://doi.org/10.1002/2015JD024092, 2015b.

Xie, S., Terai, C., Wang, H., Tang, Q., Fan, J., Burrows, S., Lin, W., Wu, M., Song, X., Zhang, Y., Taylor, M., Golaz, J.-C., Benedict, J., Chen, C.-C., Feng, Y., Hannah, W., Ke, Z., Shan, Y., Larson, V., and Bader, D.: The Energy Exascale Earth System Model Version 3. Part I: Overview of the Atmospheric Component, Under Review, https://doi.org/10.22541/essoar.174456922.21825772/v1, 2025.

Yukimoto, S., Kawai, H., Koshiro, T., Oshima, N., Yoshida, K., Urakawa, S., Tsujino, H., Deushi, M., Tanaka, T., Hosaka, M., Yabu, S., Yoshimura, H., Shindo, E., Mizuta, R., Obata, A., Adachi, Y., and Ishii, M.: The meteorological research institute Earth system model version 2.0, MRI-ESM2.0: Description and basic evaluation of the physical component, Journal of the Meteorological Society of Japan, 97, 931–965, https://doi.org/10.2151/jmsj.2019-051, 2019.

Yumimoto, K., Tanaka, T. Y., Oshima, N., and Maki, T.: JRAero: The Japanese Reanalysis for Aerosol v1.0, Geoscientific Model Development, 10, 3225–3253, https://doi.org/10.5194/gmd-10-3225-2017, 2017.

Zender, C. S. and Kwon, E. Y.: Regional contrasts in dust emission responses to climate, Journal of Geophysical Research Atmospheres, 110, https://doi.org/10.1029/2004JD005501, 2005.

Zender, C. S., Bian, H., and Newman, D.: Mineral Dust Entrainment and Deposition (DEAD) model: Description and 1990s dust climatology, Journal of Geophysical Research: Atmospheres, 108, https://doi.org/10.1029/2002jd002775, 2003.

Zhang, J., Teng, Z., Huang, N., Guo, L., and Shao, Y.: Surface renewal as a significant mechanism for dust emission, Atmospheric Chemistry and Physics, 16, 15 517–15 528, https://doi.org/10.5194/acp-16-15517-2016, 2016.

Zhao, A., Ryder, C. L., and Wilcox, L. J.: How well do the CMIP6 models simulate dust aerosols?, Atmospheric Chemistry and Physics, 22, 2095–2119, https://doi.org/10.5194/acp-22-2095-2022, 2022.

Zomer, R. J., Xu, J., and Trabucco, A.: Version 3 of the Global Aridity Index and Potential Evapotranspiration Database, Scientific Data, 9, https://doi.org/10.1038/s41597-022-01493-1, 2022.

Zou, X. K. and Zhai, P. M.: Relationship between vegetation coverage and spring dust storms over northern China, Journal of Geophysical Research: Atmospheres, 109, https://doi.org/10.1029/2003jd003913, 2004.